



# Tensile strength of unsaturated coarse and fine-grained soils

S. Bulolo<sup>1</sup> · E. C. Leong<sup>1</sup> · R. Kizza<sup>1</sup>

Received: 4 August 2020 / Accepted: 6 December 2020 / Published online: 20 January 2021  
© Springer-Verlag GmbH Germany, part of Springer Nature 2021

## Abstract

Soils at the ground surface experience multiple cycles of drying and wetting. On drying, the soils experience shrinkage and cracks may appear. The development of cracks depends on the tensile strength of the soil. Such cracks increase the permeability of the soil and can cause slopes and earth structures to fail due to rainfall. Several tensile strength models have been proposed for unsaturated soils considering the effect of matric suction. However, the tensile strength models proposed are for either cohesionless (coarse-grained) or clayey (fine-grained) soils. The tensile strength models were shown to be different in their definition of suction stress and the presence or absence of a cohesion term. As tensile strength data of fine-grained soils with the same soil structure and soil–water characteristic curve (SWCC) data are lacking in the literature, Brazilian tensile tests and SWCC tests were conducted on compacted fine-grained soils from two residual soil formations. The test data highlighted the problem in the friction angle used in existing tensile strength models. Using a general form of the suction stress and the extended Mohr–Coulomb criterion with the Brazilian test Mohr circle, a new tensile strength model applicable to both coarse-grained and fine-grained soils was proposed. The proposed model was shown to perform better than existing models using independent data.

**Keywords** Tensile strength · Brazilian test · Matric suction · Unsaturated soils

## Introduction

Soils near the ground surface experience multiple drying and wetting cycles according to weather and climatic conditions. As soil dries, it experiences shrinkage and tensile cracks. These cracks affect the integrity of soil structures such as slopes, dams, and embankments in terms of permeability and strength. Cracks in the soil provide an easy pathway for rainwater infiltration and such phenomenon is commonly associated with failures in slopes, dams, and earth structures. Tensile cracks are highly influenced by the tensile strength of soils (Morris et al. 1992; Trabelsi et al. 2012; Vaniceek 2013; Shi et al. 2014; Li et al. 2019; Tang et al. 2019). Research shows that the tensile strength of unsaturated soils is mainly influenced by matric suction of the unsaturated soils (De Souza Villar et al. 2009; Yin and Vanapalli 2018).

Tensile strength tests for soils are generally grouped based on the method of load application: direct and indirect tensile tests. Direct tensile strength tests usually involve constraining one of the boundaries of the test specimen and applying uniaxial tensile force to the opposite boundary. The direct tensile test is regarded as the only method where a specimen is subjected to true uniaxial tension and failure occurs along its longitudinal axis (Peters and Leavell 1988; Win 2006). In a direct tensile test, it is assumed that uniform stresses are applied to the specimen, and torsional and bending stresses are absent. The tensile strength is computed as a ratio of the maximum load sustained by the specimen and the cross-sectional area on which the load acts. Direct tensile strength tests have been conducted on soils (Tschebotarioff et al. 1953; Hasegawa and Ikeuti 1966; Ajaz and Parry 1975; Peters and Leavell 1988; Tang and Graham 2000; Trabelsi et al. 2010; Li et al. 2019; Murray and Tarantino 2019).

Despite the advantages of direct tensile strength test, the validity of the tests has been questioned due to difficulties associated with the test such as difficulty to effectively clamp or hold the specimen at the ends, misalignment, stress concentration, and eccentric loading (Kennedy and Hudson 1968). Creep and volume changes as a result of sustained loading during the test have also been reported (Win 2006).

---

✉ E. C. Leong  
cecileong@ntu.edu.sg

<sup>1</sup> School of Civil & Environmental Engineering, Nanyang Technological University, Blk N1, 50 Nanyang Avenue, Singapore 639798, Singapore

To address some of the difficulties in direct tensile tests, indirect tensile tests have been developed. Although the failure mode in indirect tensile test is a combination of compression and tension, indirect tensile tests have several advantages over direct tensile tests. It is relatively simple, failure is located in a region of uniform tensile strength, the specimens and equipment are the same as the compression tests, the surface conditions of the specimen do not affect the failure, and there is less variation of the test results (Kennedy and Hudson 1968). Many studies have been conducted on soils using indirect tensile tests (e.g., Uchida and Matsumoto 1961; Kennedy and Hudson 1968; Khrihnyaya and Eisenstein 1974; Al-Hussaini 1981; Dexter and Kroesbergen 1985; Das et al. 1995; Li and Wong 2013; Akin and Likos 2017; Pittaro 2019). Among the indirect tensile tests, the Brazilian tensile strength (BTS) test is the most frequently used (Khrihnyaya and Eisenstein 1974; Das et al. 1995; Vesga and Vallejo 2006; De Souza Villar et al. 2009; Beckett et al. 2015; Irvanian and Bilsel 2016; Akin and Likos 2017). Comparison between direct and indirect tensile tests shows no significant differences between the tensile strength (e.g., Vesga and Vallejo 2006; Fahimifar and Malekpour 2012; Kim et al. 2012).

Several tensile strength models for unsaturated soils considering the effects of matric suction have been proposed. However, the tensile strength model is either for cohesionless (coarse-grained) soils or clayey (fine-grained) soils. Generally, tensile strength models considering the effects of matric suction have been developed for coarse-grained soils rather than for fine-grained soils and hence tensile strength data together with soil–water characteristic curve data for fine-grained soils are scarce in the literature. In some literature, unsaturated soils were prepared by compacting a soil at various water contents to the same dry density, but the soils prepared in this manner have a different soil structure. Such data are not used in the present study.

The present study aims to develop a tensile strength model considering the effect of matric suction for both coarse and fine-grained soils. As tensile strength data for fine-grained soils with the same soil structure and soil–water characteristic curve data are lacking in the literature, the present study includes Brazilian tensile strength tests on fine-grained soils initially compacted wet of optimum and allowed to dry to various water contents. The matric suctions of the compacted soil specimens were measured using the contact filter paper method (ASTM D5298–16 2016) as well as estimated from its soil–water characteristic curve (ASTM D6836-16 2016).

## Tensile strength models

Several theoretical models (Fisher 1926; Morris et al. 1992; Lu et al. 2009; Varsei et al. 2016) and empirical models (Kim and Hwang 2003; Munkholm and Kay 2014; Yin and

Vanapalli 2018; Wang et al. 2020) have been developed to predict the tensile strength of soils. Tensile strength models based on the macromechanics approach compared to the micromechanical approach are more attractive for practical applications (Yin and Vanapalli 2018). A summary of the tensile strength models based on the macromechanics approach is presented in Table 1. In Table 1, the models of Morris et al. (1992), Trabelsi et al. (2012), Tang et al. (2015), and Varsei et al. (2016) were developed for clayey soils while the models of Lu et al. (2009), Yin and Vanapalli (2018), and Wang et al. (2020) were developed for cohesionless soils. In most of the models shown in Table 1, the tensile strength  $\sigma_t$  of unsaturated soils is usually obtained from the Mohr–Coulomb criterion with the  $y$ -axis intercept given by the apparent cohesion  $c_{app}$  as shown in Fig. 1. The  $\sigma_t$  is obtained from either direct uniaxial tensile test or indirect tensile test. If the uniaxial tensile test is used, the Mohr circle will have the minor principal stress as  $-\sigma_t$  and major principal stress as 0. Based on Fig. 1, this case will give

$$\begin{aligned}\sigma_t &= \frac{2\cos\phi_t}{1 + \sin\phi_t} c_{app}^*; \text{ or alternatively } \sigma_t \\ &= 2\tan\left(\frac{\pi}{4} - \frac{\phi_t}{2}\right) c_{app}^*\end{aligned}\quad (1)$$

The parameters of  $\phi_t$  and  $c_{app}^*$  are defined in Fig. 1.

If an indirect tensile test such as the Brazilian tensile test (ASTM D3967–16 2016) is used, the Mohr circle will have the minor principal stress as  $-\sigma_t$  and the major principal stress as about  $3.1\sigma_t$  (Li and Wong 2013; Sivakugan et al. 2014; Consoli et al. 2015). In this case,  $\sigma_t$  is given by Eq. 2.

$$\sigma_t = \frac{\cos\phi'}{(2.05 - 1.05\sin\phi')} c_{app}\quad (2)$$

The parameters of  $\phi'$  and  $c_{app}$  are defined in Fig. 1.

Except for Snyder and Miller (1985) in Table 1, the other tensile strength models can be expressed in the form of either Eq. 1 or 2 where  $c_{app}$  can be expressed in the form of the total cohesion in the extended Mohr–Coulomb criterion for unsaturated soils (Fredlund et al. 1978) as shown in Eq. 3.

$$c_{app} = c' + (u_a - u_w)\tan\phi^b\quad (3)$$

where  $c'$  is the effective cohesion,  $u_a$  is pore air pressure,  $u_w$  is pore water pressure, and  $\phi^b$  is the angle indicating the rate of shear strength increase due to matric suction ( $u_a - u_w$ ). Equation 3 can also be expressed more generally in term of a suction stress  $\sigma^s$  as shown in Eq. 4.

$$c_{app} = c' + \sigma^s \tan\phi^b\quad (4)$$

**Table 1** Summary of tensile strength models with consideration of matric suction using the macroscopic approach

Reference	Tensile strength model's equations
Snyder and Miller (1985)	$\sigma_t = \frac{1}{f(s)} \chi (u_a - u_w)$ <p>where <math>\sigma_t</math>=tensile stress, <math>f(s)</math>=proportionality factor based on stress concentration of Griffith (1924) fracture criterion and is a function of the degree of saturation, <math>\chi</math>=Bishop's chi factor, <math>u_a</math>= pore air pressure, and <math>u_w</math>=pore water pressure</p>
Morris et al. (1992)	$\sigma_t = 0.5[c' + (u_a - u_w) \tan \phi^b]$ based on Frydman (1967) and Baker (1981) or $\sigma_t = (0.5 \text{ to } 0.7)[c' + (u_a - u_w) \tan \phi^b] \cot \phi'$ based on Bagge (1985) where $c'$ and $\phi'$ =effective shear strength parameters, $\phi^b$ =angle indicating rate of shear strength increase with respect to matric suction
Lu et al. (2009)	$\sigma_t = \left[ 2, \tan \left( \frac{\pi - \phi_t}{4} \right) \right] \sigma^s \tan \phi$ <p>where</p> $\sigma^s = \begin{cases} u_w & \text{for } (u_a - u_w) \leq 0 \\ S_e (u_a - u_w) & \text{for } (u_a - u_w) \geq 0 \end{cases}$ $S_e = \frac{S - S_r}{1 - S_r}$ <p><math>(u_a - u_w) = \frac{1}{\alpha} [S_e^{n/(1-n)} - 1]^{1/n}</math> - Van Genuchten (1980) SWCC equation  <math>S</math>=degree of saturation, <math>S_e</math>=effective degree of saturation, <math>S_r</math>=residual degree of saturation, <math>\alpha</math> and <math>n</math>=van Genuchten SWCC equation parameters</p>
Trabelsi et al. (2012)	$\sigma_t = \frac{2 \cos \phi'}{1 + \sin \phi'} \cdot \{ \sigma_s \tan \phi' + C^* \}$ , where $\sigma_s = \frac{A}{\tan \phi'} \cdot \left( \frac{ f(n^*)  + f(n^*)}{2} \right) (u_a - u_w)$ $C^* = B \cdot \left( \frac{ f(n^*)  + f(n^*)}{2} \right)$ $f(n^*) = 1 - \left( \frac{n^*}{n^*_0} \right)^p$ <p><math>A, B</math>=parameters, <math>n^*</math>=porosity, <math>n^*_0</math>=reference porosity, and <math>p</math>=material parameter characterizing the shape of the cohesion-porosity function</p>
Tang et al. (2015)	$\sigma_t = \begin{cases} \left[ 2 \tan \left( \frac{\pi - \phi_t}{4} \right) \right] \sigma^s \tan \phi_t & 0 \leq S \leq S^c \\ \left[ 2 \tan \left( \frac{\pi - \phi_t}{4} \right) \right] \sigma^s \tan \phi_t + \sigma_{tr} & S^c \leq S \leq 100\% \end{cases}$ <p>where  <math>\sigma^s = S_e (u_a - u_w)</math>  <math>(u_a - u_w) = \frac{1}{\alpha} [S_e^{n/(1-n)} - 1]^{1/n}</math>  <math>\sigma_{tr}</math>= residual tensile strength and <math>S^c</math> = critical degree of saturation</p>
Varsei et al. (2016)	$\sigma_t = \frac{2 \cos \phi'}{1 + \sin \phi'} [\sigma_s \tan \phi' + c']$ <p>where  <math>\sigma_s = S_e^m (u_a - u_w)</math>,  <math>S_e^m = \frac{S - S_r^m}{1 - S_r^m} = (S)^{\alpha^*}</math>  <math>S_r^m</math> = microscopic degree of saturation and <math>\alpha^*</math>=material parameter (always greater than 1)</p>
Yin and Vanapalli (2018)	$\sigma_t = \left[ 2, \tan \left( \frac{\pi - \phi_t}{4} \right) \right] \sigma^s \tan \phi$ <p>where</p> $\sigma^s = S_e^k (u_a - u_w) + T_s a_{aw}$ $k = \begin{cases} \frac{1}{(n-1)} \frac{1}{1 - [(0.85 \pm 0.15) S_c]^{n/n-1}} & \text{for } C_u \leq 6 \\ \frac{1}{(n-1)} \frac{1}{1 - [(0.45 \pm 0.15) S_c]^{n/n-1}} & \text{for } C_u > 6 \end{cases}$ $\frac{S_0}{S_c} = \begin{cases} (0.85 \pm 0.15) & \text{for } C_u \leq 6 \\ (0.45 \pm 0.15) & \text{for } C_u > 6 \end{cases}$ $a_{aw} = \eta_s \frac{\pi}{e d_{50}} S_e^{\lambda_s} (1 - S_e)$ $\eta_s = 0.73 C_u$ $\lambda_s = \frac{S_r}{1 - S_r}$ <p><math>C_u</math>=coefficient of uniformity, <math>S_c</math>=capillary degree of saturation, <math>S_0</math>=degree of saturation corresponding to the peak tensile strength induced by capillary suction, <math>e</math>=void ratio, <math>d_{50}</math>=diameter at 50% passing</p>

**Table 1** (continued)

Reference	Tensile strength model's equations
Wang et al. (2020)	$\sigma_t = \left[ 2_t \tan \left( \frac{\pi}{4} - \frac{\phi_t}{2} \right) \right] \sigma^s \tan \phi$ <p>where</p> $\sigma^s = S_e(u_a - u_w) + T_s a_{aw}$ $(u_a - u_w) = \alpha \left( S_e^{\frac{n}{n-1}} - 1 \right)^{\frac{1}{n}}$ $\alpha = \frac{12.07 T_s}{d_{60}}$ $n = \frac{1.07}{\log_{10} C_u} + 1;$ $a_{aw} = \eta_s \frac{\pi}{e d_{50}} S_e^{\lambda_s} (1 - S_e)$ $\eta_s = 0.73 C_u$ $\lambda_s = 0.3$

In the tensile strength model of Morris et al. (1992), the coefficient of 0.5 based on Frydman (1967) and Baker (1981) and the coefficient of (0.5 to 0.7)  $\cot \phi'$  based on Bagge (1985) shown in Table 1 can be examined in the context of Eqs. 1 and 2. Figure 2 shows a plot of coefficient  $\left( \frac{2 \cos \phi_t}{1 + \sin \phi_t} \right)$  from Eq. 1 and coefficient  $\left[ \frac{\cos \phi'}{(2.05 - 1.05 \sin \phi')} \right]$  from Eq. 2 versus the friction angle  $\phi_t$  or  $\phi'$  for the typical range from 15 to 50°. It can be seen that the coefficient  $\left( \frac{2 \cos \phi_t}{1 + \sin \phi_t} \right)$  is close to  $0.7 \cot \phi'$  for the range of  $\phi' = \phi_t$  from 28 to 40° and the coefficient  $\left[ \frac{\cos \phi'}{(2.05 - 1.05 \sin \phi')} \right]$  is close to 0.5 for the full range of friction angle.

For the other tensile strength models in Table 1, Eq. 1 is used and only differs in the definition of  $\sigma^s$  and the presence or absence of a cohesion term. The tensile strength models of

Tang et al. (2015), Yin and Vanapalli (2018), and Wang et al. (2020) originated from Lu et al. (2009). The differences among these models lie in the definition of  $\sigma^s$  which can be expressed in the general form of Eq. 5.

$$\sigma^s = S_e^k (u_a - u_w) + f \tag{5}$$

where  $S_e$  is the effective degree of saturation  $\left( = \frac{S - S_r}{1 - S_r} \right)$ ,  $S_r$  is the residual degree of saturation, and exponent  $k$  is a parameter. The first term on the right-hand side of Eq. 5 is attributed to capillary suction while the second term ( $f$ ) is attributed to surface tension of the “capillary bridges” (Yin and Vanapalli 2018; Wang et al. 2020). Only the exponent  $k$  in Yin and Vanapalli (2018) model is not unity. Yin and Vanapalli (2018) relate  $k$  to be a function of van Genuchten (1980) soil–water characteristic curve (SWCC) equation parameter

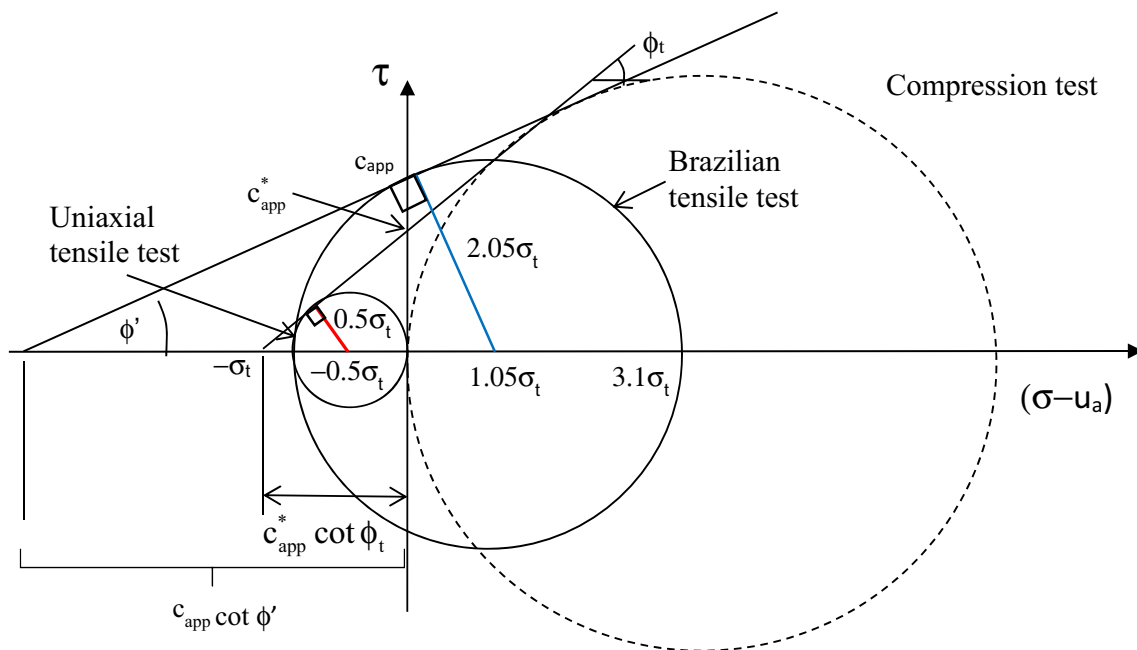


**Figure 1** Representations of uniaxial and Brazilian tensile strength tests using Mohr–Coulomb failure criterion

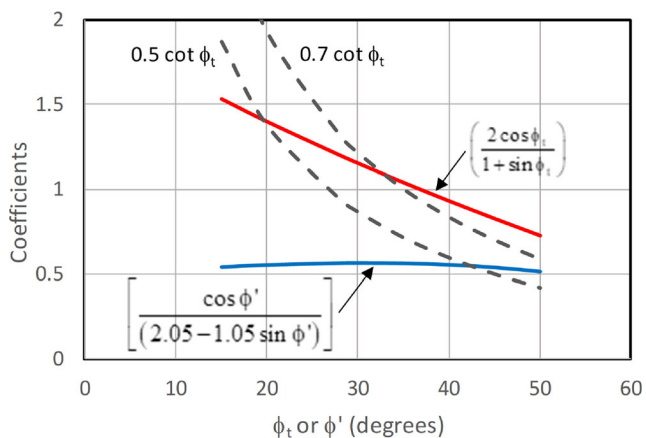


**Fig. 2** Comparison of coefficients in Eqs. 1 and 2 with Morris et al. (1992) model

$n$  and capillary degree of saturation  $S_c$  which is dependent on the coefficient of uniformity  $C_u$ . The equations are shown in Table 1. The effective degree of saturation  $S_e$  is defined differently in Varsei et al. (2016) who make use of a microscopic degree of saturation  $S_r^m$  following Alonso et al. (2010) instead of residual degree of saturation  $S_r$  as shown in Eq. 6.

$$S_e^m = \frac{S - S_r^m}{1 - S_r^m} = (S)^{\alpha^*} \tag{6}$$

Instead of determining  $S_r^m$ , Varsei et al. (2016) proposes Eq. 7 where  $\alpha^*$  is a material parameter and is always equal to or greater than 1.

$$S_e^m = (S)^{\alpha^*} \tag{7}$$

The term  $f$  is zero in Lu et al. (2009), Trabelsi et al. (2012), Tang et al. (2015), and Varsei et al. (2016). Wang et al. (2020) followed Yin and Vanapalli’s (2018) formulation of  $f$  to be a product of surface tension of water  $T_s$  and the specific air–water interfacial area per pore volume  $a_{aw}$ , i.e.,  $f = T_s \cdot a_{aw}$ . The equations are given in Table 1.

Lu et al. (2009), Tang et al. (2015), Yin and Vanapalli (2018), and Wang et al. (2020) make use of the van Genuchten (1980) SWCC equation in their tensile strength model. However, Wang et al. (2020) propose equations to determine the van Genuchten (1980) SWCC equation parameters  $\alpha$  and  $n$ , as shown in Table 1.

As the models of Lu et al. (1992), Yin and Vanapalli (2018), and Wang et al. (2020) were developed for cohesionless soils, the cohesion term is zero. However, three out of ten soils that Yin and Vanapalli (2018) used in the development of their model are fine-grained soils. In contrast, the models of Trabelsi et al. (2012), Tang et al. (2015), and Varsei et al. (2016) were developed for clayey soils and hence contain a cohesion term. Only Varsei et al. (2016) kept the cohesion term as the effective cohesion. In Trabelsi et al. (2012) model, the cohesion term is

a function of porosity while in the Tang et al. (2012) model, the cohesion is given by the residual tensile strength at full saturation. However, Tang et al.’s (2015) model was developed for soils compacted at various water contents to the same dry density. Thus, Tang et al.’s (2015) model assumes that the influence of the soil structure on  $\sigma_t$ ,  $\alpha$ , and  $n$  is negligible.

In summary, the macroscopic approach tensile strength models showed variations only in the definition of the suction stress  $\sigma^s$  and the presence of a cohesion term  $c$  for clayey soils only. The general form of the macroscopic approach tensile strength model is expressed in Eq. 8.

$$\sigma_t = 2 \tan\left(\frac{\pi}{4} - \frac{\phi}{2}\right) (\sigma_s \tan \phi + c) \tag{8}$$

The suction stress  $\sigma^s$  consists of either one term (Lu et al. 2009; Tang et al. 2015; Varsei et al. 2016) or two terms (Yin and Vanapalli 2018; Wang et al. 2020).

In the development of the tensile strength model for unsaturated soils, the grain size distribution curve, SWCC, and effective shear strength parameters for the saturated soil,  $c'$  and  $\phi'$ , are required. The tensile strength tests should also be performed for a soil either undergoing drying or wetting process and not on soils prepared at various water contents to avoid effects of soil structure on the test results. Tensile strength test data with SWCC are more commonly found for coarse-grained (cohesionless) soils than for fine-grained (clayey) soils in the literature, hence tensile strength tests and SWCC tests are performed for fine-grained soils in the present study.

**Table 2** Basic properties of the soils used in study

Soil	BT	JF
LL (%)	58	43
PL (%)	31	24
$G_s$	2.63	2.71
$d_{10}$ (mm)	0.00150	0.00014
$d_{30}$ (mm)	0.002	0.002
$d_{50}$ (mm)	0.005	0.02
$d_{60}$ (mm)	0.009	0.1
Coefficient of uniformity, $C_u$	6.0	714.3
Coefficient of curvature, $C_c$	0.296	0.286
USCS	MH	CL
Standard Proctor		
Maximum dry density (Mg/m <sup>3</sup> )	1.69	1.76
Optimum water content (%)	16.0	16.0
Modified Proctor		
Maximum dry density (Mg/m <sup>3</sup> )	1.86	1.94
Optimum water content (%)	13.3	13.5

## Materials and methods

### Soil materials

Two residual soils, one from the Bukit Timah Granite (BT) and the other from the Jurong Formation (JF) in Singapore, were used as the fine-grained soils in the present study. The Bukit Timah Granite is mainly an acidic igneous rock system while the Jurong Formation is predominantly a folded sedimentary rock system (Leong et al. 2002b). The basic properties of the two residual soils are summarized in Table 2.

The standard (SP) and modified Proctor (MP) compaction curves of the residual soils according to ASTM D698 - 12e2 (2015) and ASTM D1557-12e1 (2015), respectively, are shown in Fig. 3. The maximum dry densities for the standard Proctor effort for BT and JF are 1.69 and 1.76 Mg/m<sup>3</sup>, respectively, corresponding to an optimum water content of 16% for both soils. The maximum dry densities for the modified Proctor effort for BT and JF are 1.86 and 1.94 Mg/m<sup>3</sup>, corresponding to optimum water contents of 13.3 and 13.5%, respectively. The compaction properties of BT and JF residual soils are also included in Table 2. The preparation of the samples is described below.

**Fig. 3** Compaction curves and sample sets

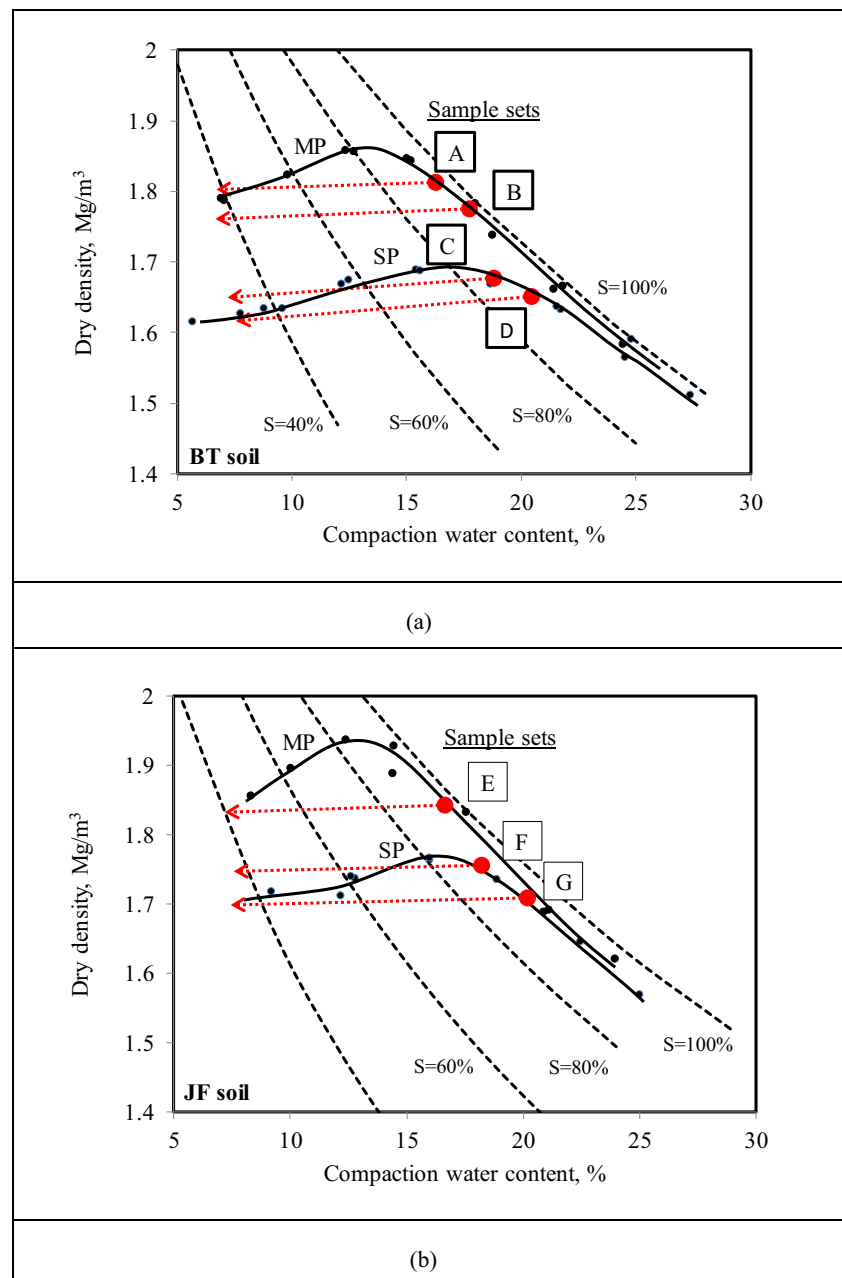
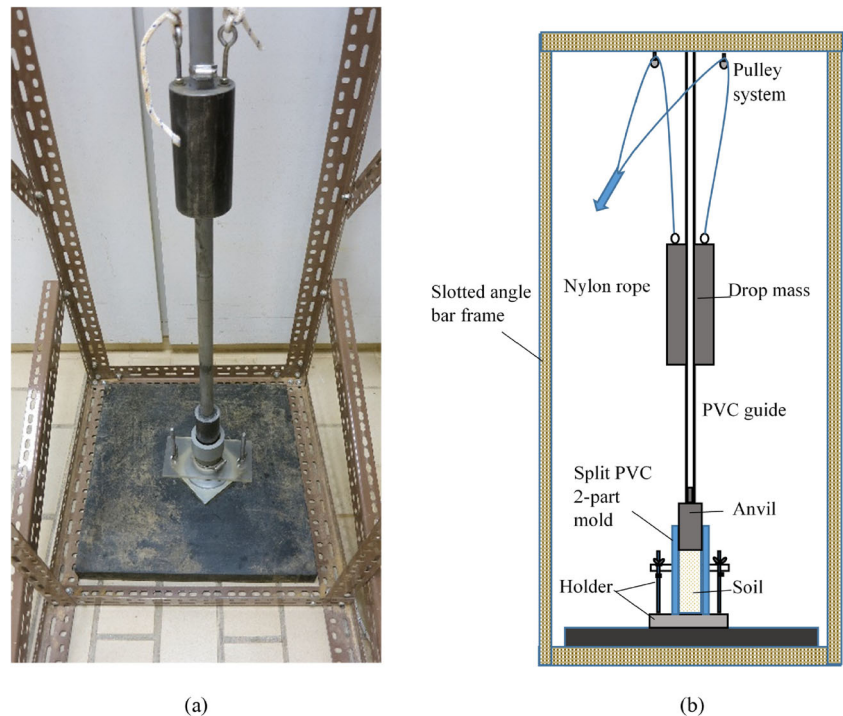




**Fig. 4** Compaction set-up to prepare soil specimens in PVC mold



## Sample preparation and test procedures

### Compaction

The air-dried residual soils were passed through sieve no. 4 and mixed with distilled water to the target moisture contents. The soils were then sealed in Ziploc bags and stored in a humidity chamber for at least 5 days to allow for moisture equalization.

To obtain test specimens of about 50 mm in diameter for the BTS test, a two-part split PVC cylindrical mold (internal diameter of 52 mm and height of 102 mm) was fabricated. A compaction apparatus was fabricated to ensure that the compaction procedure is consistent for the preparation of the soil samples. The compaction apparatus, shown in Fig. 4, was equipped with a pulley system to lift a cylindrical drop mass of 4.5 kg and dimensions of 75 mm diameter and 150 mm

height with a center hole. The drop mass center hole slides along a PVC tube guide which is slotted onto a dowel on top of a solid steel cylinder, diameter 51.6 mm and height of about 100 mm, which acts as the anvil. The anvil is placed on top of the soil in the PVC two-part split mold. A PVC collar sits on top of the PVC two-part split mold to constrain the anvil. The PVC two-part split mold is held together with hose clips and rests on the standard compaction mold base plate. The PVC two-part split mold is held upright at mid-height by an acrylic square plate with a center hole that is held in place using the screws of the standard compaction mold base plate and nuts. The height of fall of the drop mass was calibrated to deliver standard and modified Proctor energies to the soil. For the standard Proctor energy, the drop mass falls through a height of 200 mm and the soil is compacted in three layers while for the modified Proctor energy, the drop mass falls through a height of 450 mm and the soil is compacted in five layers. For both compaction energies, each layer in the PVC mold was subjected to six blows. The compacted sample produced has a height of about 100 mm.

Before each compaction, the internal walls of the PVC split mold were lightly oiled. During compaction, each layer was scarified before placing another layer to allow for bonding between the layers. The soils were compacted wet of optimum on both the standard and modified Proctor curves, indicated as A to D for BT soils and E to G for JF soils in Fig. 3a and b, respectively. As each of these points are compacted at different water contents wet of optimum, the soil structure is different and thus each point can be said to be a “different” soil. For each point, A to G, multiple samples were prepared and

**Table 3** Properties of sample sets A to G

Soil	Sample set	Average, $w$ (%)	Average, $\rho_d$ (Mg/m <sup>3</sup> )	Proctor effort
BT	A	16.0	1.82	Modified
	B	17.5	1.77	Modified
	C	18.0	1.72	Standard
	D	20.5	1.68	Standard
JF	E	17.0	1.84	Modified
	F	18.0	1.75	Standard
	G	20.0	1.70	Standard

collectively, these samples are denoted as sample sets A to G and the average soil properties are summarized in Table 3.

### Brazilian tensile strength (BTS) test

Tensile strength of soil is commonly determined in the laboratory by direct and indirect tensile test methods. Although the indirect tensile test has been criticized as being less reliable, research has shown that the indirect tensile tests have advantages over the direct tensile test such as indirect tensile test is relatively simpler to perform; the specimens and equipment can be the same as for compression tests; the failure is located in a region of uniform tensile strength; the surface condition of the specimen does not affect the failure and there is less variability in the test results (Al-Hussaini and Townsend 1973; Vaniceek 2013; He et al. 2018).

The Brazilian tensile strength (BTS) test is an indirect tensile test originally developed for rock (ASTM D3967–16 2016) but has been used to obtain the tensile strength of soils (e.g., Krishnayya and Eisenstein 1974; Das et al. 1995; Vesga and Vallejo 2006; De Souza Villar et al. 2009; Beckett et al. 2015; Iravani and Bilsel 2016; Akin and Likos 2017). A review on the development of the BTS test can be found in Li and Wong (2013). In the BTS test, the applied load is compressive but the failure mode is tensile if specific constraints on specimen geometry (thickness to diameter,  $t/d$ , and ratio) are met. In ASTM D3967–16 2016, the  $t/d$  ratio is recommended to be within the range of 0.2 to 0.75. Akin and Likos (2017) found that the tensile strength is essentially constant when  $t/d$  ratio is greater than 0.42 for kaolin. In the present study, the  $t/d$  ratio of the test specimens was maintained as close to 0.6 as possible. Hence, each compacted sample of 100 mm length was sawn using Buehler IsoMet™ 4000 precision saw into three cylindrical disk specimens of about 30 mm thick and 52 mm in diameter. Although the precision saw can minimize sample deformation and have

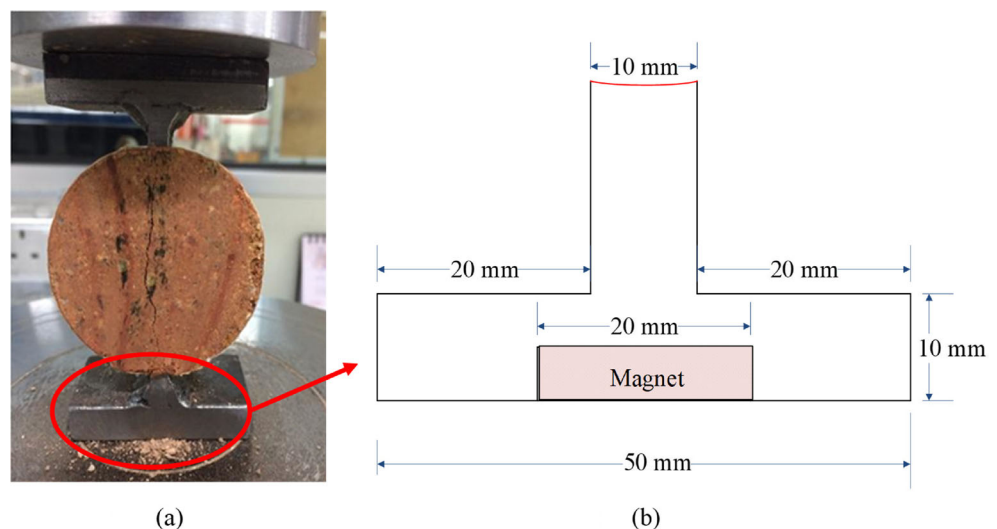
low kerf loss, the compacted sample was wrapped in two layers of cling film followed by a single layer of masking tape along the sample height to prevent moisture loss and to limit surface cracking during sawing. The disk specimens were then dried to various water contents in airtight desiccators with saturated sodium chloride (NaCl) solution at the base of the desiccators. The saturated NaCl solution provides a constant relative humidity of about 76% (Young 1967) to dry the test specimens. Weight and volume of the disk specimens were measured regularly to provide the shrinkage curve. Test specimens that attained the targeted weight (and hence moisture content) were wrapped in cling film and thereafter kept in a temperature-controlled humidity chamber to allow for moisture equalization for about 10 days as recommended by Mendes (2011) before testing.

The test specimens for the BTS in the present study were loaded using two specially fabricated curved bearing blocks as recommended in ASTM D3967–16 2016 to reduce contact stress. The radius of the contact arc and width of contact with the test specimen were 10° and 30 mm, respectively. During testing, the bearing blocks were attached to the loading platens of an unconfined compression test machine using magnets embedded into the base of the bearing block (Fig. 5). The BTS test was conducted at a loading rate of 0.5 mm/min and all test specimens failed within 1 to 10 min as recommended in ASTM D3967–16 2016. The tensile strength  $\sigma_t$  was computed from the BTS test results using Eq. 9 (ASTM D3967–16 2016).

$$\sigma_t = 1.272 \frac{P}{\pi t D} \quad (9)$$

where  $P$  is the maximum applied load in the BTS test,  $t$  is the thickness of the specimen, and  $D$  is the diameter of the specimen. The number of tensile tests conducted for each sample set ranges from 35 to 66 giving a total of 343 tensile test results. Observations during the BTS tests show that crack

**Fig. 5** Brazilian test set-up and curved bearing block





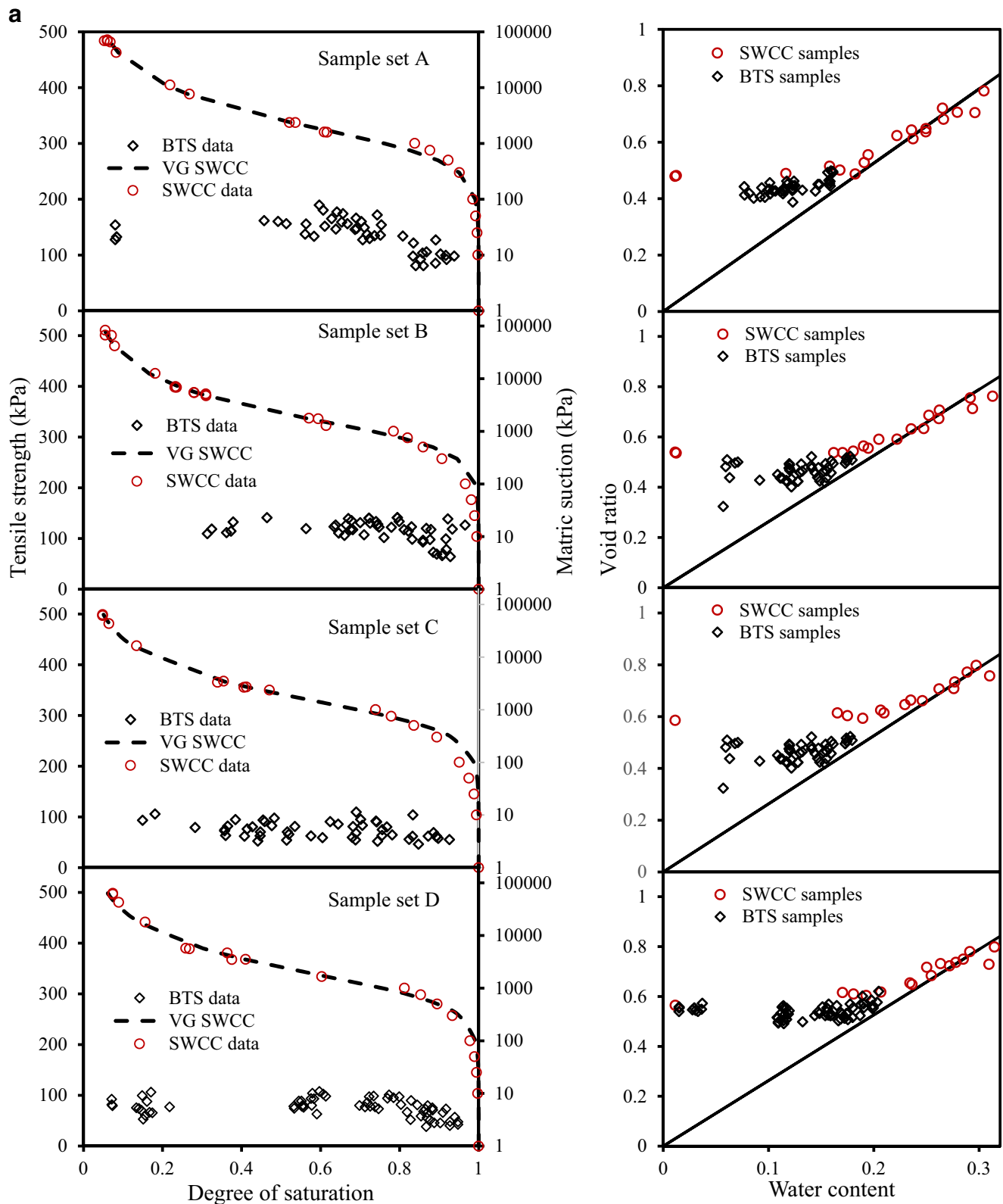


**Fig. 6** a Summary of test results for sample sets A to D. b Summary of test results for sample sets E to G

initiated at the center of the disk and the stress–displacement curves exhibited brittle failure in almost all the tests indicating

the general applicability of the BTS test for the compacted soils in the present study (Frydman 1964, 1967).

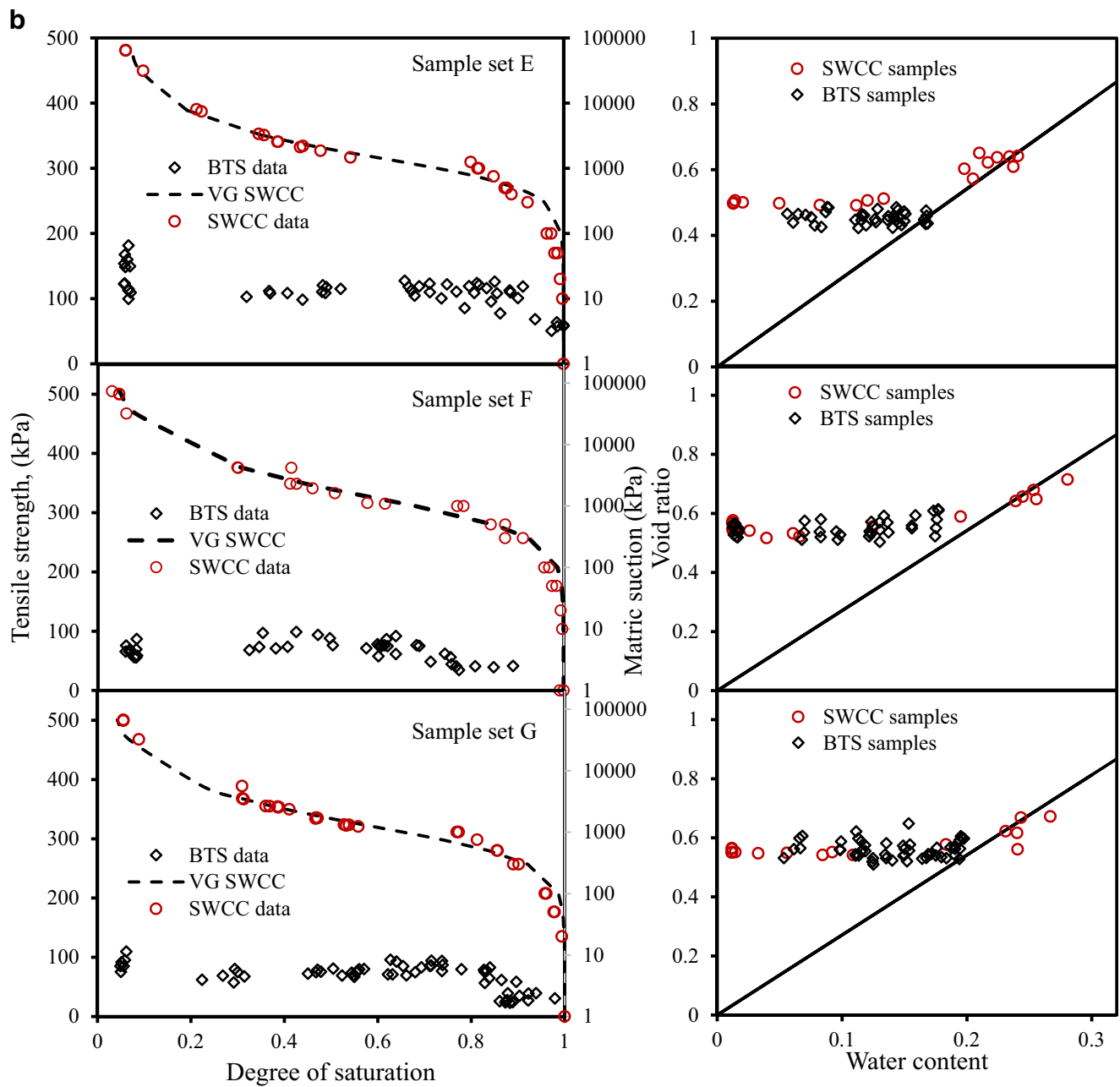
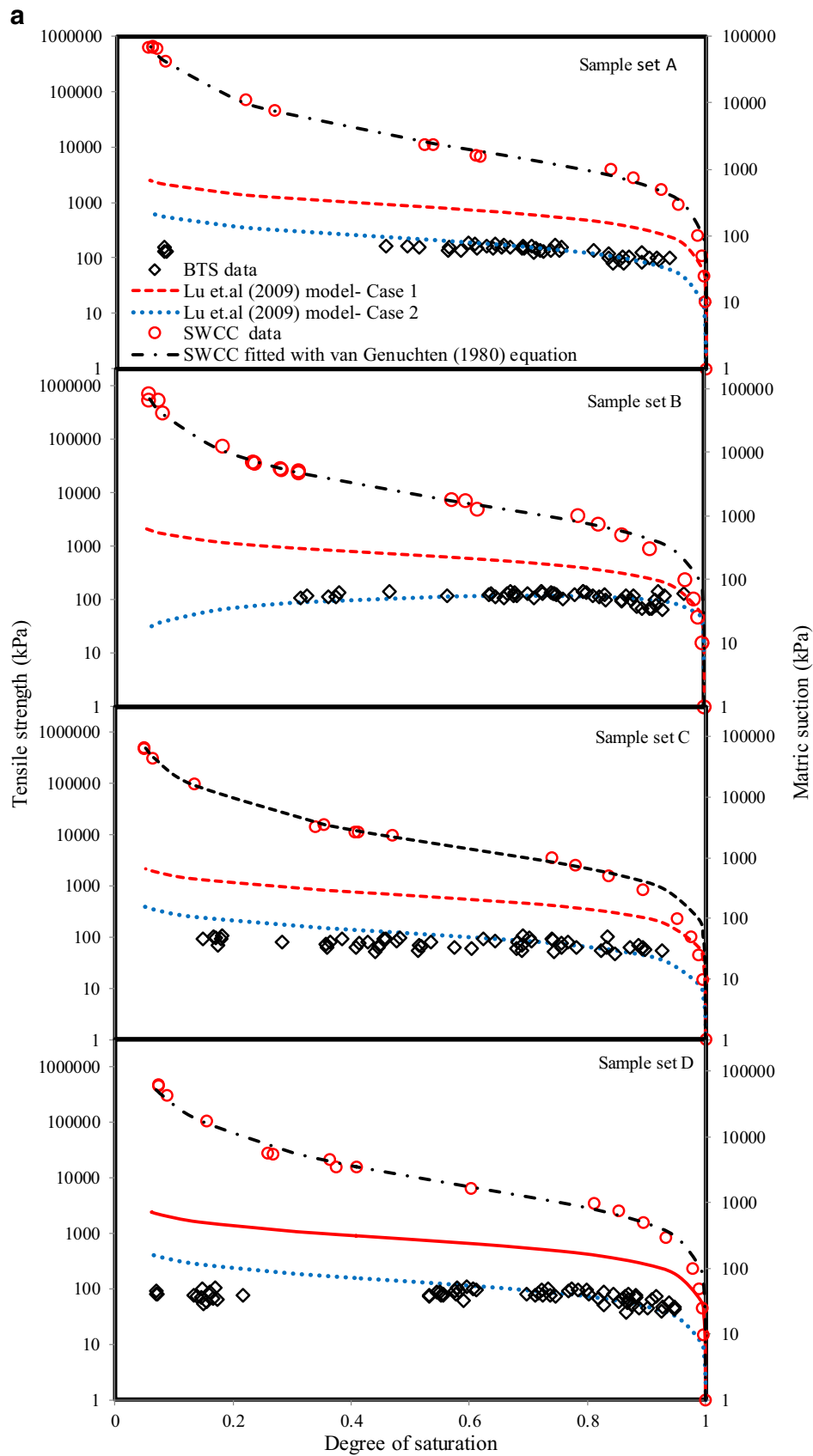


Fig. 6 (continued)

**Table 4** Shear strength and SWCC equations' parameters for sample sets A–G

Sample set	From CU tests with pore-water pressure measurements		van Genuchten (1980) SWCC equation's parameters	
	$\phi'$ (°)	$c'$ (kPa)	$\alpha$ (kPa <sup>-1</sup> )	$n$
A	27.3	8	0.0010	1.670
B	28.2	10	0.0011	1.715
C	28.6	2	0.0013	1.682
D	27.5	5	0.0010	1.675
E	30.0	10	0.0010	1.949
F	29.0	10	0.0013	1.671
G	26.0	10	0.0014	1.737



**Fig. 7** **a** Evaluation of Lu et al. (2009) tensile strength model (sample sets A-D). **b** Evaluation of Lu et al. (2009) tensile strength model (sample sets E-G)

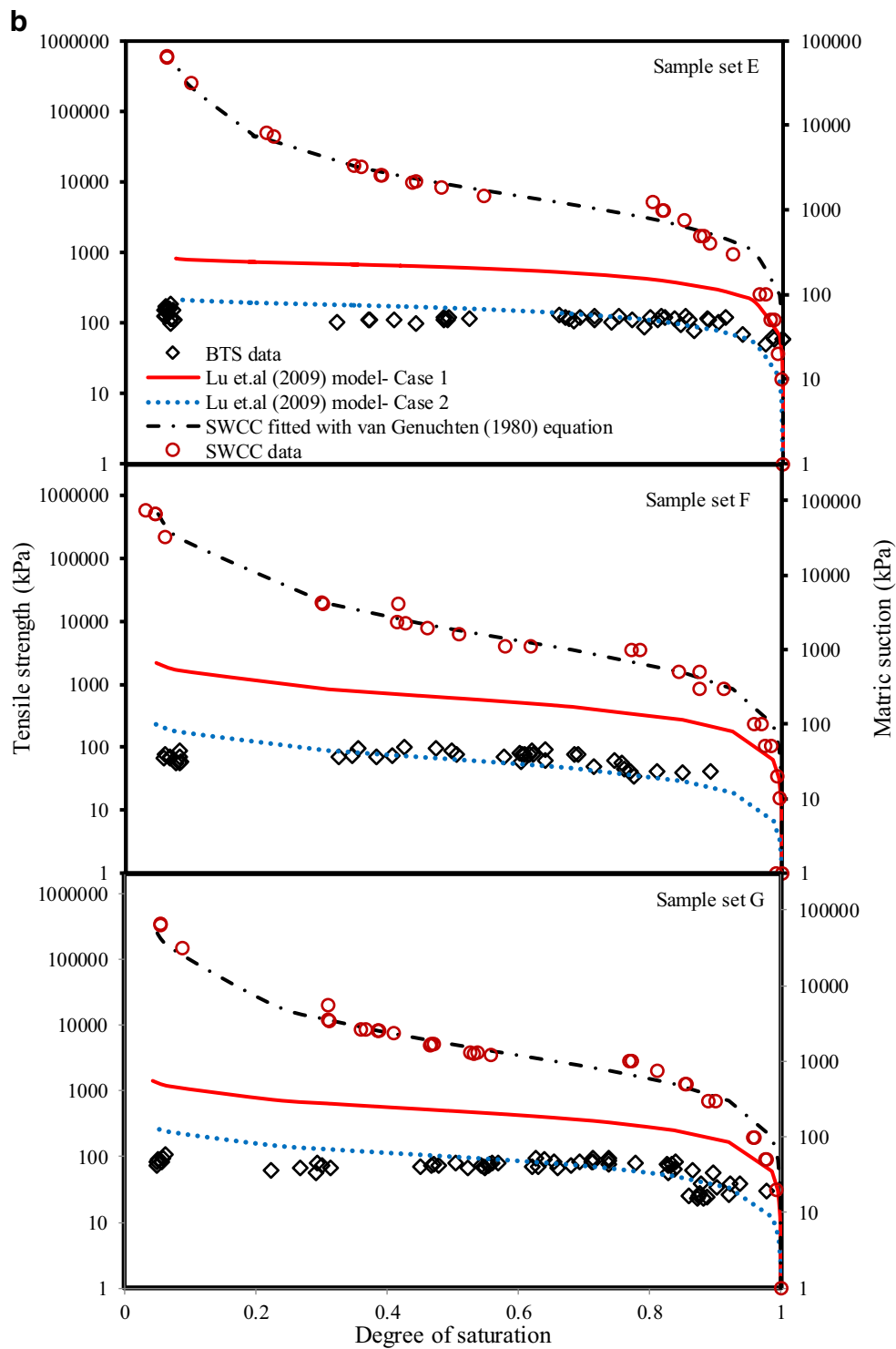


Fig. 7 (continued)

**Suction measurements**

Suction measurements were conducted on the compacted soil samples using the contact filter paper method following Leong et al. (2002a). Whatman No. 42 filter paper of diameter 42.5 mm was used. The matrix

suction calibration equations for Whatman No. 42 filter paper used were those suggested by Leong et al. (2002a) and reproduced in Eq. 10.

$$\log \psi = \begin{cases} 2.909 - 0.0229w_f, & w_f \geq 47, \\ 4.945 - 0.0673w_f, & w_f < 47 \end{cases} \quad (10)$$

**Table 5** Summary of  $\phi_t$  and RMSE for Lu et al. (2009) tensile strength model

Sample set	Case 1		Case 2	
	$\phi_t = \phi'$ (°)	RMSE	$\phi_t$ (°)—fitted	RMSE
A	27.3	682.4	10.0	109.2
B	28.2	382.2	11.0	57.4
C	28.6	580.5	7.0	58.9
D	27.5	835.8	7.0	101.8
E	30.0	476.7	4.0	53.2
F	29.0	918.4	2.0	58.9
G	26.0	506.3	2.0	61.7

where  $\psi$  is the matric suction and  $w_f$  is the water content of the filter paper in percent.

For the suction measurement, the compacted soil sample was sawn into four cylindrical disk specimens of about 25 mm height each. A piece of filter paper was sandwiched between two disk specimens and then wrapped in cling film and taped to minimize moisture loss as suggested by Bulut et al. (2001). Each of the taped specimens was then placed in an airtight container and kept in a constant temperature chamber for 28 days to allow for suction equilibration. At the end of 28 days, procedures recommended by Bulut et al. (2001) were followed to determine the water content  $w_f$  of the filter paper. The matric suction of the compacted soil was then computed using Eq. 10.

### Soil–water characteristic curves

The SWCCs of the compacted soils were established using both the pressure plate apparatus (method C) and the chilled-mirror dewpoint technique (method D) following ASTM D6836-16 (2016). For suctions up to and including 1000 kPa, a pressure plate apparatus with a 15-bar ceramic plate cell was used. For suctions higher than 1000 kPa, the WP4C dewpoint potentiometer (Leong et al. 2003) was used.

Before commencement of the pressure plate test, the compacted samples were saturated following the procedure suggested by Agus et al. (2001) and then disk specimens of 50 mm diameter and 30 mm height were used. The suction level in the pressure plate extractor was increased incrementally from 10 to 1000 kPa as recommended in ASTM D6836-16 (2016). At equilibrium, the weight and volume of the specimens were measured to provide the shrinkage curve.

For the WP4C dewpoint potential meter, a cylindrical disk specimen of diameter 35 mm and thickness 5 mm was cookie-cut from the saturated compacted sample using a PVC ring with a sharpened edge and placed into the WP4C sample cups. These specimens in the sample cups were dried in airtight

desiccators containing saturated NaCl solution. The weights of the sample cups with the soils were monitored periodically as the soil dries and concurrently, the suction was measured using the WP4C dewpoint potentiometer. The drying continued until no further change in weight could be observed (less than 0.001 g). The sample cups with the soils were then left outside the desiccator (laboratory environment at  $22 \pm 4$  °C and relative humidity at  $\sim 60\%$ ) to allow for further drying and measuring the suction using the WP4C dewpoint potentiometer until no further weight change could be detected (less than 0.001 g).

## Results and discussion

### Tensile strength tests

The test results for sample sets A to D and E to F are summarized in Fig. 6 a and b, respectively. For all the sample sets, drying of the soil specimens from the wet of optimum to dry of optimum showed an increase in  $\sigma_t$ . The  $\sigma_t$  values increase up to a certain limit and then generally becomes constant despite further drying or increase in soil suction. Some data show a slight drop in  $\sigma_t$  at extremely low water contents. The degree of saturation at which  $\sigma_t$  ceases to increase significantly varies between 95 and 97% for all the sample sets. Locating these degrees of saturation on the shrinkage curves indicates that they correspond approximately to the curvature of the shrinkage curve, which begins to depart from the 100% degree of saturation line and approaches the minimum void ratio. As the soil dries, its volume decreases and suction increases. These factors collectively influence  $\sigma_t$ . However, the contribution of suction to  $\sigma_t$  becomes increasingly minimal past the air-entry value (AEV) of the soil since the water phase becomes increasingly discontinuous in the soil. Hence,  $\sigma_t$  ceases to increase and becomes almost constant when the shrinkage limit is reached. Any deviation from the constant value is attributed to micro-fissures in the specimen and can be classified as experimental errors.

### Evaluation of tensile strength models

Review of the tensile strength models showed a general form and two variations of suction stress which can be represented by the models of Lu et al. (2009) and Yin and Vanapalli (2018).

For evaluation of the tensile strength models,  $\phi'$  is needed. The  $\phi'$  values for sample sets A to G were obtained from consolidated undrained triaxial tests for saturated soil specimens of each sample set conducted following ASTM D4767-11 (2011) (details are reported in Kizza 2019). The effective stress shear strength parameters ( $c'$  and  $\phi'$ ) and the van



**Table 6** Summary of parameters and RMSE for Yin and Vanapalli et al.'s (2018) tensile strength model

Sample set	Parameters and RMSE	Case 1 $\phi_t = \phi'$	Case 2 $\phi_t$ —fitted	Other model parameters
A	$\eta_s$	4.38	4.38	$e=0.45$
	$k$	3.72	3.72	$d_{50}=0.005$ mm
	$\phi'$	27.3°	10	$S_c=0.91$
	$\lambda_s$	0.001	0.001	$S_r=0.0010$
	RMSE	159.0	27.2	
B	$\eta_s$	4.38	4.38	$e=0.48$
	$k$	3.52	3.52	$d_{50}=0.005$ mm
	$\phi'$	28.2°	11	$S_c=0.92$
	$\lambda_s$	0.014	0.014	$S_r=0.0140$
	RMSE	86.4	40.5	
C	$\eta_s$	4.38	4.38	$e=0.515$
	$k$	3.61	10.78	$d_{50}=0.005$ mm
	$\phi'$	28.6°	7	$S_c=0.90$
	$\lambda_s$	0.001	0.001	$S_r=0.0010$
	RMSE	82.6	46.1	
D	$\eta_s$	4.38	4.38	$e=0.49$
	$k$	3.64	3.64	$d_{50}=0.005$ mm
	$\phi'$	27.5°	7	$S_c=0.91$
	$\lambda_s$	0.001	0.001	$S_r=0.0010$
	RMSE	82.5	39.4	
E	$\eta_s$	73	73	$e=0.44$
	$k$	1.49	1.49	$d_{50}=0.02$ mm
	$\phi'$	30°	4	$S_c=0.90$
	$\lambda_s$	0.06	0.06	$S_r=0.0580$
	RMSE	221.9	69.6	
F	$\eta_s$	73	73	$e=0.44$
	$k$	1.90	1.90	$d_{50}=0.02$ mm
	$\phi'$	29°	2	$S_c=0.90$
	$\lambda_s$	0.0001	0.0001	$S_r=0.0001$
	RMSE	215.62	42.57	
G	$\eta_s$	73	73	$e=0.505$
	$k$	1.77	1.77	$d_{50}=0.02$ mm
	$\phi'$	26°	2	$S_c=0.92$
	$\lambda_s$	0.0066	0.0066	$S_r=0.0065$
	RMSE	174.59	46.84	

Genuchten (1980) SWCC equation parameters ( $\alpha$  and  $n$ ) for sample sets A to G are tabulated in Table 4.

Lu et al. (2009) suggest that  $\phi_t$  be obtained using a non-linear Mohr–Coulomb envelope in the low-stress zone and can be greater than the effective friction angle  $\phi'$  (see Fig. 1). For the presentation of results, two cases of  $\phi_t$  values are shown, i.e.

Case 1. All parameters were as evaluated from experimental data, i.e.,  $\alpha$  and  $n$  of the van Genuchten (1980) SWCC equation from curve fitting the SWCC data while  $\phi_t = \phi'$  as given in Table 4.

Case 2. Values of  $\alpha$  and  $n$  of the van Genuchten (1980) SWCC equation as for case 1 while  $\phi_t$  was adjusted to obtain the best match with the experimental data.

The performance of Lu et al. (2009) tensile strength model is shown in Fig. 7 a. In Fig. 7 a, the SWCC is also plotted. To evaluate the performance of the tensile strength model against the experimental data, the root mean square error (RMSE) was computed. The RMSE is defined in Eq. 11.

$$RMSE = \sqrt{\frac{\sum_{i=1}^n (X_{obs,i} - X_{model,i})^2}{n}} \quad (11)$$

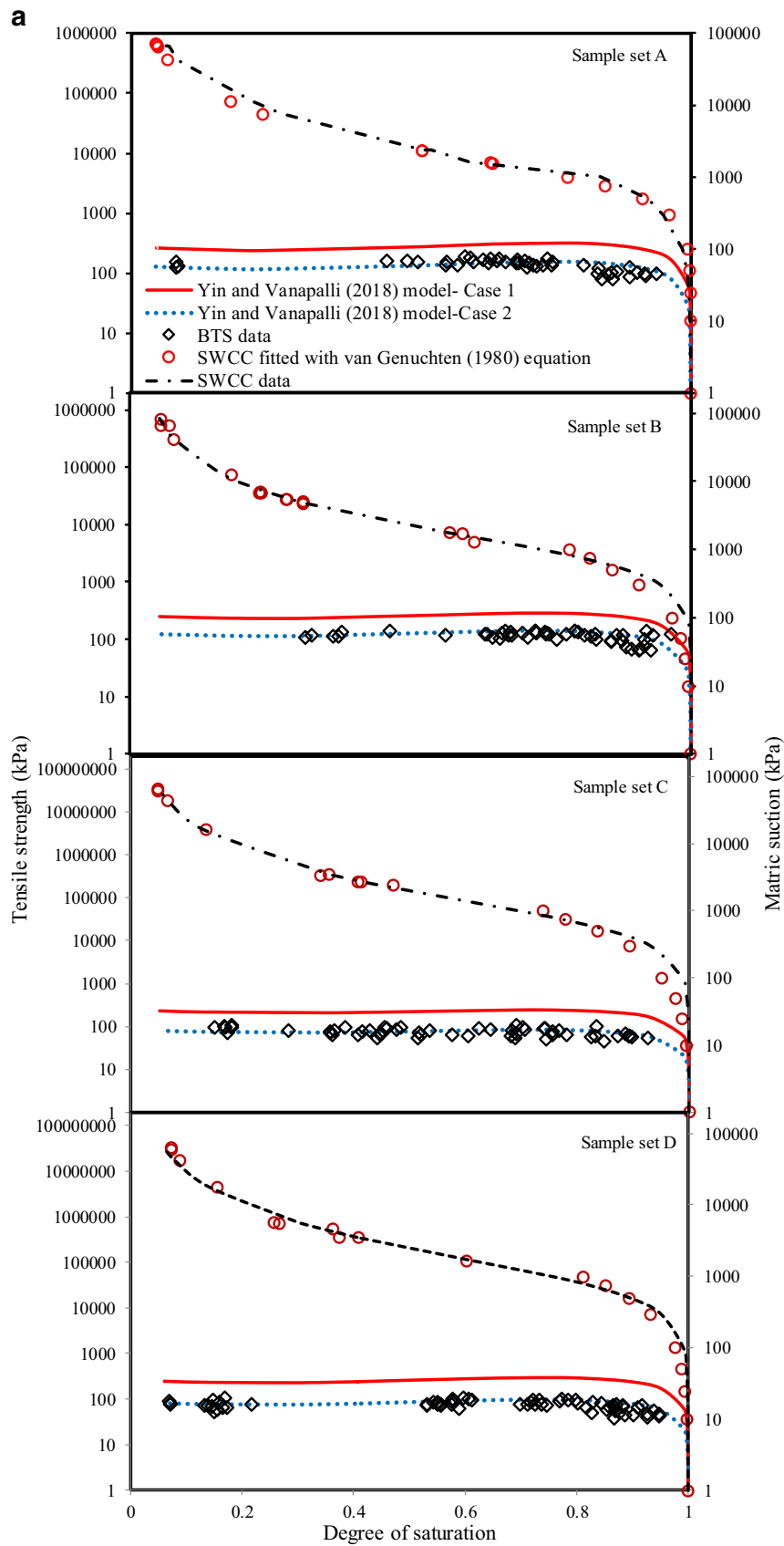


**Fig. 8 a** Evaluation of Yin and Vanapalli (2018) tensile strength model (sample sets A–D). **b** Evaluation of Yin and Vanapalli (2018) tensile strength model (sample sets E–G)

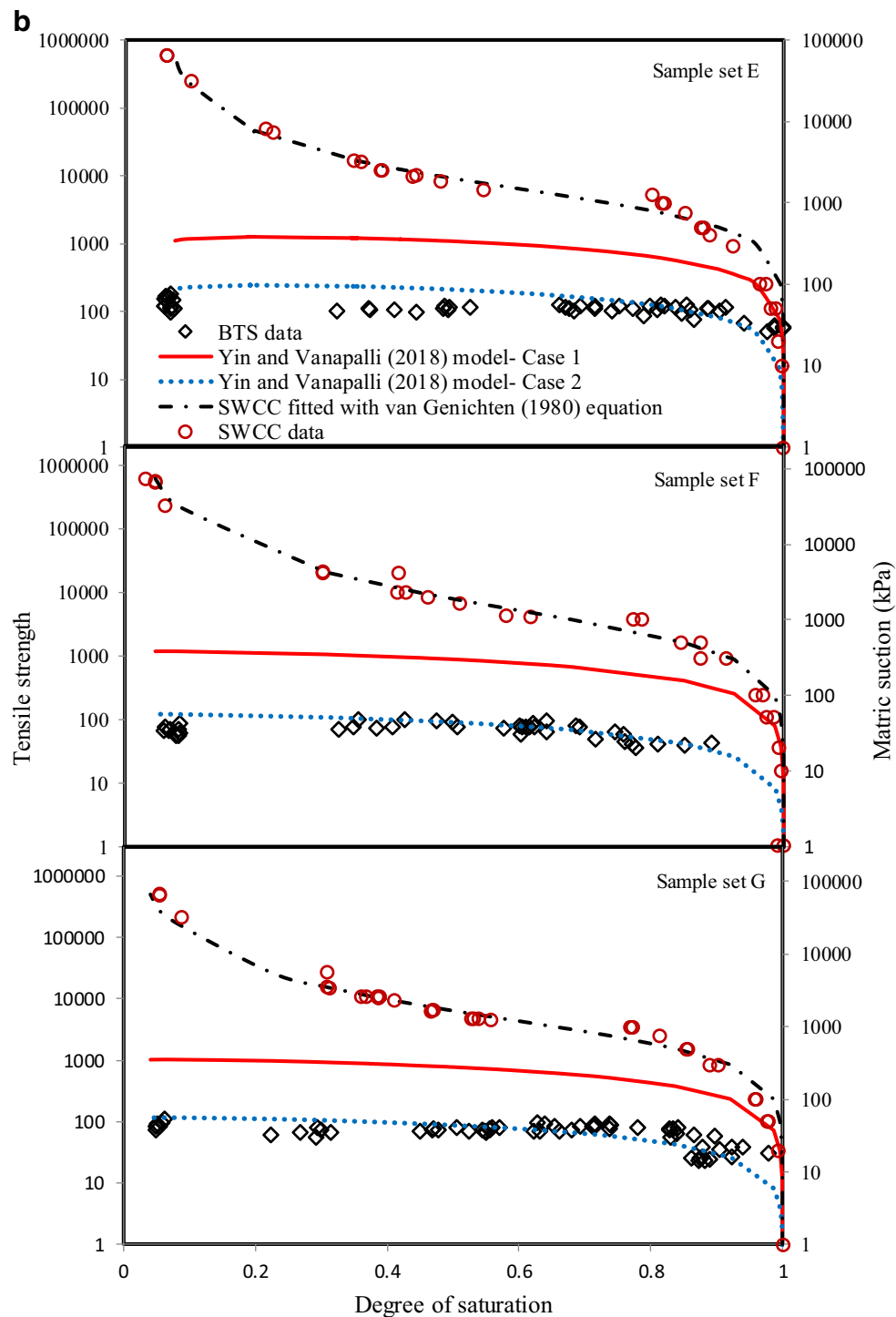


Fig. 8 (continued)

where  $X_{\text{obs}, i}$  = observed/measured value,  $X_{\text{model}, i}$  = model value as predicted at the same conditions as observed value, and  $n$  = number of data points. A smaller RMSE indicates a better agreement.

As expected, case 2 gives the better estimate as compared to case 1 for all sample sets A to G. The values of  $\alpha$  and  $n$  of the van Genuchten (1980) SWCC

equation seem too low for Lu et al. (2009) tensile strength model to estimate the test data. In case 2, the value of  $\phi_t$  needs to be reduced from  $\phi'$  to get a better match with the test data, but there is no justification for the reduction in  $\phi_t$ . Table 5 summarizes the  $\phi_t$  and RMSE values for all the sample sets A to G. If a cohesion term was included in Lu et al.'s (2009) tensile

**Table 7** Parameters used in the development of the proposed tensile strength model

Reference	Soil type	$\phi'$ (°)	$c'$ (kPa)	$\alpha$ (kPa <sup>-1</sup> )	$n$	$S_c$	$S_r$	$e$	$d_{50}$ (mm)	$C_u$	$C_c$	$P_{200}$ (%)
Test dataSet A	Fine grained (MH)	27.3	8	0.0009	1.710	0.91	0.001	0.45	0.005	6.00	0.296	72
Test dataSet B	Fine grained (MH)	28.2	10	0.0010	1.725	0.92	0.014	0.48	0.005	6.00	0.296	72
Test dataSet C	Fine grained (MH)	28.6	2	0.0013	1.682	0.90	0.0	0.52	0.005	6.00	0.296	72
Test dataSet D	Fine grained (MH)	27.5	5	0.0012	1.675	0.91	0.001	0.49	0.005	6.00	0.296	72
Test dataSet E	Fine grained (CL)	30.0	10	0.0012	1.949	0.90	0.058	0.44	0.020	714.29	0.286	58
Test dataSet F	Fine grained (CL)	29.0	10	0.0014	1.671	0.90	0.0	0.44	0.020	714.29	0.286	58
Test dataSet G	Fine grained (CL)	26.0	10	0.0014	1.757	0.92	0.007	0.51	0.020	714.29	0.286	58
Goulding (2006)	F-75 Dense sand	27.3	0	0.3011	4.527	0.95	0.015	0.65	0.210	1.733	0.926	39
	F-75 Loose sand	27.3	0	0.2741	4.527	0.95	0.015	0.75	0.210	1.73	0.926	39
	F-55 Dense sand	28.0	0	0.3960	4.261	0.95	0.001	0.65	0.250	1.5	0.996	24
	F-55 Loose sand	28.0	0	0.3960	4.361	0.93	0.001	0.75	0.250	1.5	0.996	24
	F-40 Dense sand	30.0	0	0.3050	5.002	0.94	0.001	0.65	0.330	1.52	0.825	15
	F-40 Loose sand	30.0	0	0.3050	5.002	0.92	0.001	0.75	0.330	1.52	0.825	15
Lu et al. (2007)	Silty sand	48.0	0	0.2500	3.750	0.92	0.020	0.82	0.110	1.83	0.742	96
	Fine sand	48.0	0	0.1811	3.409	0.94	0.048	0.82	0.170	1.31	0.652	83
Lu et al. (2009)	Medium sand	48.0	0	0.7091	3.760	0.93	0.001	0.67	0.450	1.52	0.747	0
	Esperance sand	48.0	0	0.8295	4.109	0.92	0.093	0.82	0.230	2.00	0.781	40
Narvaez et al. (2015)	Tailing A (ML)	35.2	0	0.0056	2.145	0.91	0.0	0.84	0.012	9.5	1.684	98
	Tailing B (ML)	35.0	0	0.0125	2.468	0.92	0.010	0.79	0.030	14	2.294	99
	Tailing C (ML)	35.0	0	0.0018	2.100	0.92	0.001	0.81	0.021	20.00	0.800	100

strength model, the value of  $\phi_t$  would need to be further reduced to achieve a good match with the test data.

Similar to Lu et al.'s (2009) tensile strength model, Yin and Vanapalli's (2018) tensile strength model could not estimate the test data well. For the presentation of results, two cases that gave the best estimate of the test data are presented:

- Case 1. The parameters  $k$  and  $\eta_s$  were computed using the equations in Table 1 while  $\phi_t = \phi'$ .
- Case 2. The parameters  $k$  and  $\eta_s$  were as for case 1, while  $\phi_t$  was adjusted to give the best match with the experimental data.

The void ratio  $e$  in Eq. 8 is taken to be  $e_{min}$  from the shrinkage curve (Leong and Wijaya (2015)). For the computation of  $k$ , the ratio  $S_0/S_c$  was set at 0.9 and 0.6 for BT and JF soils, respectively, within the range of values given by Yin and Vanapalli (2018).

Figure 8a shows the two cases where  $\sigma_t$  is plotted against  $S$  for all the sample sets A to G together with their SWCCs. Table 6 summarizes the parameters and the RMSE values for all the sample sets A to G. As expected, case 2 gives the lower RMSE for all the sample sets. Similar to Lu et al.'s (2009) tensile strength model,  $\phi_t$  in Yin and Vanapalli (2018) model needs to be reduced from  $\phi'$  to obtain a better match with the test data and a further reduction is needed if a cohesion term is included in Yin and Vanapalli (2018) model. The model requires the use of either larger values of  $k$  and  $\eta_s$  or a smaller  $\phi_t$  value to get a better match.

In both Lu et al.'s (2009) and Yin and Vanapalli's (2018) tensile strength models, a better estimate of  $\sigma_t$  can only be obtained by using  $\phi_t < \phi'$  as shown in Tables 5 and 6. This is undesirable as  $\phi_t$  becomes a fitting parameter and the model cannot be used in the predictive sense. Hence, a more suitable tensile strength

**Table 8** Correlation matrix for coarse-grained soils

Parameter	$\alpha$	$n$	$e$	$d_{50}$	$C_u$	$C_c$	$P_{200}$ (%)	$\alpha \cdot C_u$	$\alpha \cdot C_c$	$n \cdot C_u$	$n \cdot C_c$	$e \cdot P_{200}$	$e \cdot n$
A	-0.0922	0.0677	-0.5721	0.0231	-0.1077	0.9247	-0.4212	-0.1441	0.1568	0.0441	0.2954	-0.4791	-0.1210
$k_1$	0.0737	-0.5950	0.4269	-0.2261	-0.2739	-0.6682	0.4884	0.0740	-0.0531	-0.6723	-0.7230	0.5096	0.0741
$k_{1,2}$	0.1316	-0.7070	0.5667	-0.3692	-0.1289	-0.5765	0.6072	0.1368	0.0226	-0.7391	-0.7890	0.6351	0.1451

**Table 9** Correlation matrix for fine-grained soils

Parameter	$\alpha$	$n$	$e$	$d_{50}$	$C_u$	$C_c$	$P_{200}$ (%)	$\alpha \cdot C_u$	$\alpha \cdot C_c$	$n \cdot C_u$	$n \cdot C_c$	$e \cdot P_{200}$	$e \cdot n$
A	0.9416	0.9568	0.8165	0.4889	-0.3912	0.9859	0.7942	-0.3126	0.9246	-0.3820	0.9815	0.8237	0.9107
$k_1$	-0.7812	-0.8649	-0.8982	-0.5768	0.3166	-0.8554	-0.8163	0.1937	-0.7471	0.3197	-0.8422	-0.8814	-0.9189
$k_{1-2}$	-0.7950	-0.9198	-0.8685	-0.5613	0.3507	-0.8763	-0.8321	0.2750	-0.7733	0.3406	-0.8664	-0.8732	-0.9204

model needs to be developed keeping  $\phi_t = \phi'$  to get a better estimate of  $\sigma_t$ .

$$\sigma_t = \frac{\cos\phi'}{(2.05-1.05\sin\phi')} [\sigma^s \tan\phi' + c'] \tag{13}$$

### Proposed tensile strength model

#### Development

As mentioned earlier, Eq. 1 is generic to the tensile strength models of Lu et al. (2009), Trabelsi et al. (2012), Yin and Vanapalli (2018), Tang et al. (2015), Varsei et al. (2016), and Wang et al. (2020). However, the friction angle is not  $\phi'$  for the models of Lu et al. (2009), Tang et al. (2015), and Yin and Vanapalli (2018). By assuming that the extended Mohr–Coulomb criterion is tangent to the BTS test Mohr circle, Eq. 2 was adopted instead. The biggest difference in the tensile strength models lies in the definition of  $\sigma^s$ . The  $\sigma^s$  can be made more general by adopting the form given in Eq. 12.

$$\sigma^s = A \cdot S^{k_1} \cdot (u_a - u_w) \tag{12}$$

In Eq. 12, A is a constant and is function of basic soil properties; degree of saturation S is used which implies that  $S_r = 0$ ; exponent  $k_1$  is used instead of k to indicate that it is a different exponent from that used in Yin and Vanapalli (2018). Similar non-linear suction stress–matric suction relationship as given in Eq. 12 has been suggested by others, e.g., Kim et al. (2010). The proposed model is thus given by Eq. 13.

According to Yin and Vanapalli (2018), the exponent k is heavily related to the SWCC through van Genuchten (1980) SWCC equation parameter n and the capillary degree of saturation corresponding to the AEV ( $S_c$ ) and somewhat related to the grain size gradation parameter  $C_u$ . Hence, it is reasonable to suggest that  $k_1$  is a function of parameters associated with void ratio e, grain size distribution, and SWCC. It is highly likely that both A and  $k_1$  have different expressions for coarse and fine-grained soils. Hence, expressions for A and  $k_1$  were obtained separately for coarse and fine-grained soils. The soil properties used to obtain the proposed model parameters are  $\alpha$  and n of van Genuchten (1980) SWCC equation ( $S_r = 0$ ), void ratio e, gradation parameters,  $d_{50}$ ,  $C_u$  and  $C_c$ , and percentage passing no. 200 sieve,  $P_{200}$ . A summary of the soil parameters used is tabulated in Table 7. For the coarse-grained soils, Ottawa sand from Goulding (2006); Perth sand, Silty sand, and Fine sand from Lu et al. (2007); and Medium and Esperance sand from Lu et al. (2009) were used to develop the relationships for the proposed model parameters, A and  $k_1$ . For the fine-grained soils, the data reported in the present study together with the mine tailings from Narvaez et al. (2015) were used to develop the relationships for the proposed model parameters, A and  $k_1$ .

**Table 10** Parameters of validation data used in the proposed tensile strength model

Reference	Win (2006)	Kim and Sture (2008)	Jindal et al. (2016)	Zeh and Witt (2005)	Wong et al. (2017)	Murray and Tarantino (2019)
Soil type	Clayey sand	Medium sand	Silica sand	Clay	Clay	Vitreous clay
Tensile test	Direct	Direct	Uniaxial	Direct	Uniaxial	Uniaxial
$c'$ (kPa)	0.0	0.0	0	16.8	27.9	0
$\phi'$ (°)	25.0	32.0	48.0	25.0	32.3	27.8
n	1.655	4.145	4.492	1.578	2.253	2.115
$\alpha$ (kPa <sup>-1</sup> )	0.0005	0.4051	0.402	0.0007	0.0024	0.0006
$S_r$	0.0000	0.0000	0.0000	0.0000	0.0000	0.0000
e	0.53	0.80	0.61	0.80	0.72	0.53
$P_{200}$ (%)	47	0	0	98	100	55
$C_u$	50.00	1.79	1.84	23.33	5.00	64.29
$C_c$	0.81	0.83	0.89	0.80	0.288	1.14



**Table 11** Comparison of RMSE of the validation data for proposed, Lu et al. (2009), and Yin and Vanapalli (2018) tensile strength models

Reference	Proposed	Lu et al. (2009)	Yin and Vanapalli (2018)
Win (2006)	10.16	862.90	673.84
Kim and Sture (2008)	0.24	0.46	0.42
Jindal et al. (2016)	0.11	1.40	0.95
Zeh and Witt (2005)	119.36	1394.45	509.37
Wong et al. (2017)	6.65	113.68	217.56
Murray and Tarantino (2019)	89.03	243.43	235.09

To determine the relationships of parameters,  $A$  and  $k_1$ , with basic soil properties, an iterative optimization process was adopted. In the first iteration, the best-fit values of  $A$  and  $k_1$  to each dataset in the calibration dataset were determined. A correlation matrix between  $A$  and  $k_1$  with the basic soil properties and combinations ( $\alpha$ ,  $n$ ,  $e$ ,  $d_{50}$ ,  $C_c$ ,  $C_u$ ,  $P_{200}$ ,  $\alpha \cdot C_u$ ,  $\alpha \cdot C_c$ ,  $n \cdot C_u$ ,  $n \cdot C_c$ ,  $e \cdot P_{200}$ ,  $e \cdot n$ ) was determined. A regression analysis (using common functions of linear, exponential, power, and quadratic polynomial) was then performed on the parameter ( $A$  or  $k_1$ ) with the basic soil property or combination having the highest value in the correlation matrix. When more than one basic soil property or combination have the highest correlation values within 0.01, regression analysis was performed on each soil property or combination and the regression equation with the highest coefficient of determination  $R^2$  was selected. Once the regression equation was obtained for the parameter ( $A$  or  $k_1$ ), the value of the parameter was given by the regression equation while the other parameter ( $k_1$  or  $A$ ) was optimized again for each dataset of the calibration dataset. Subsequently, a regression analysis (using common functions of linear, exponential, power, and quadratic polynomial) was then performed on the other parameter. Finally, the coefficients of the regression equations obtained for parameters  $A$  and  $k_1$  are optimized with the calibration dataset to obtain the final regression equations.

The correlation matrices for the coarse-grained and fine-grained soils are shown in Tables 8 and 9, respectively. For coarse-grained soils, parameter  $A$  has the highest correlation with  $C_c$  (0.9247) while parameter  $k_1$  has the highest correlation with  $n \cdot C_c$  (-0.7230). As the correlation between parameter  $A$  and  $C_c$  is higher than the correlation between  $k_1$  and  $n \cdot C_c$ , a regression analysis was performed for parameter  $A$  with  $C_c$  as the independent variable to give Eq. 14.

$$A = 9.973(C_c)^{6.2} \quad (R^2 = 0.9010) \quad (14)$$

Using Eq. 14 to give the value of parameter  $A$  for each dataset in the calibration dataset, values of  $k_1$  were then optimized again to give  $k_{1,2}$  and a new correlation matrix was formed for  $k_{1,2}$  as shown in the last row of Table 8. The values of  $k_{1,2}$  have the highest correlation with  $n \cdot C_c$  (-0.7890). This correlation value is higher than the previous correlation

between  $k_1$  and  $n \cdot C_c$  (-0.7230). Hence, a regression equation was obtained for  $k_{1,2}$  with  $n \cdot C_c$  as the independent variable to give Eq. 15.

$$k_{1,2} = 2.835 \exp(-0.341 \cdot n \cdot C_c) \quad (R^2 = 0.7031) \quad (15)$$

Finally, the coefficients of the regression equations for parameters  $A$  and  $k_{1,2}$  (Eqs. 14 and 15, respectively) were optimized with the calibration dataset to give the final equations, Eqs. 16 and 17, respectively. Note the slight changes in coefficients between Eqs. 14 and 16 for parameter  $A$ , and between Eqs. 15 and 17 for parameter  $k_1$ .

$$A = 9.869(C_c)^{6.405} \quad (16)$$

$$k_1 = 2.643 \exp(-0.326 \cdot n \cdot C_c) \quad (17)$$

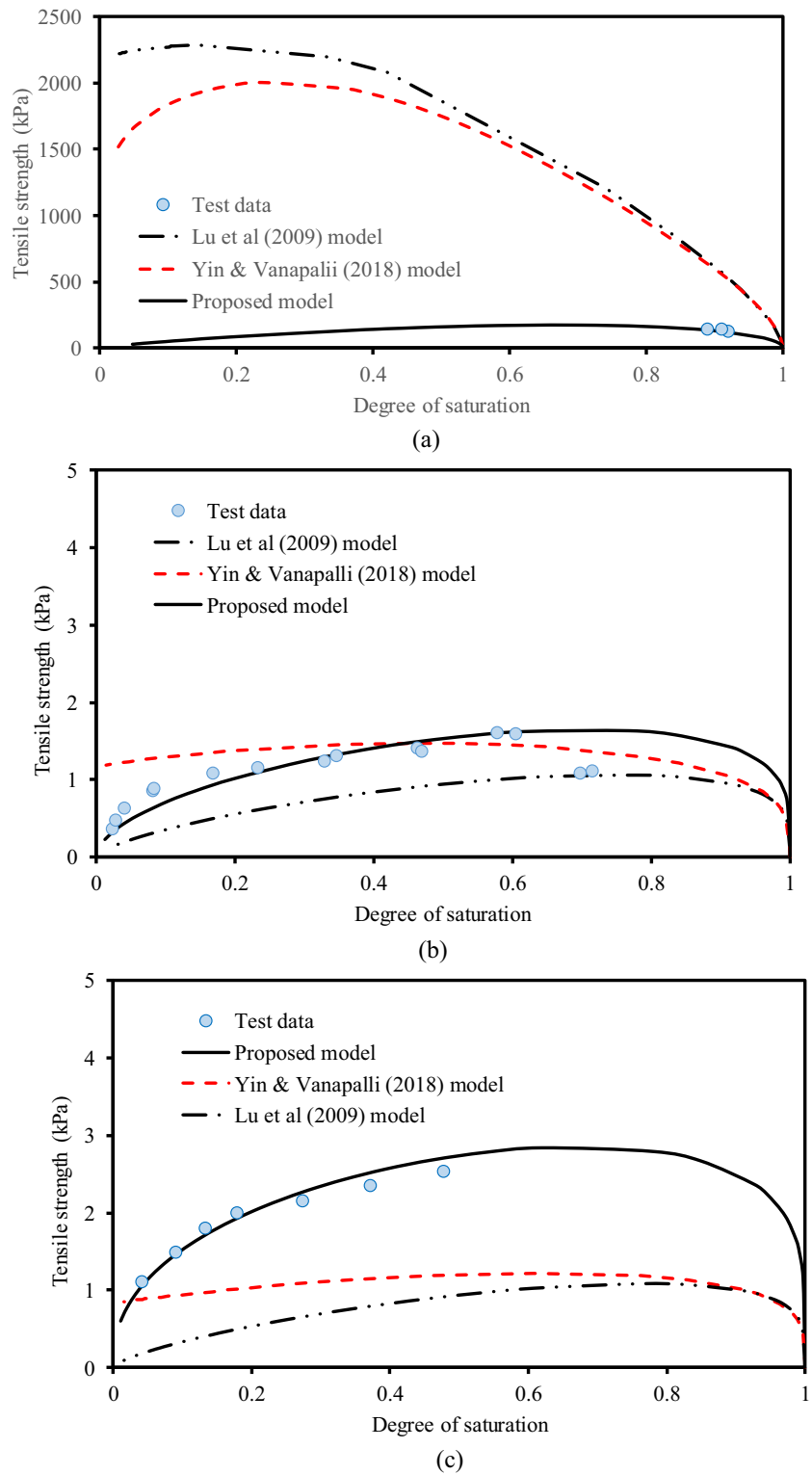
For fine-grained soils, parameter  $A$  has the highest correlations with  $C_c$  (0.9859) and  $n \cdot C_c$  (0.9815) while parameter  $k_1$  has the highest correlation with  $e \cdot n$  (-0.9289) (Table 9). As the correlations between parameters  $A$  and  $C_c$  and between parameters  $A$  and  $n \cdot C_c$  are higher than between  $k_1$  and  $e \cdot n$ , a regression analysis was performed for parameter  $A$  with  $C_c$  and  $n \cdot C_c$  as an independent variable in turn. The regression equation for parameter  $A$  adopted was the one with the highest coefficient of determination,  $R^2$ , shown in Eq. 18.

$$A = 0.0255(C_c)^2 + 0.971C_c + 0.249 \quad (R^2 = 0.9722) \quad (18)$$

Using Eq. 18 to give the value of parameter  $A$  for each dataset of the calibration dataset, the values of  $k_1$  were then optimized for the calibration dataset again to give  $k_{1,2}$  and a new correlation matrix was formed for  $k_{1,2}$  as shown in the last row of Table 9. The values of  $k_{1,2}$  have the highest correlation with  $n$  (-0.9198) and  $e \cdot n$  (-0.9294). Hence, a regression equation was obtained for  $k_{1,2}$  with  $n$  and  $e \cdot n$  as the independent variable in turn. The regression equation for  $k_{1,2}$  adopted was the one with the highest coefficient of determination,  $R^2$ , shown in Eq. 19.

$$k_{1,2} = 11.293 \exp(-1.121n) \quad (R^2 = 0.9279) \quad (19)$$

**Fig. 9** Validation of proposed tensile strength model for coarse-grained soils



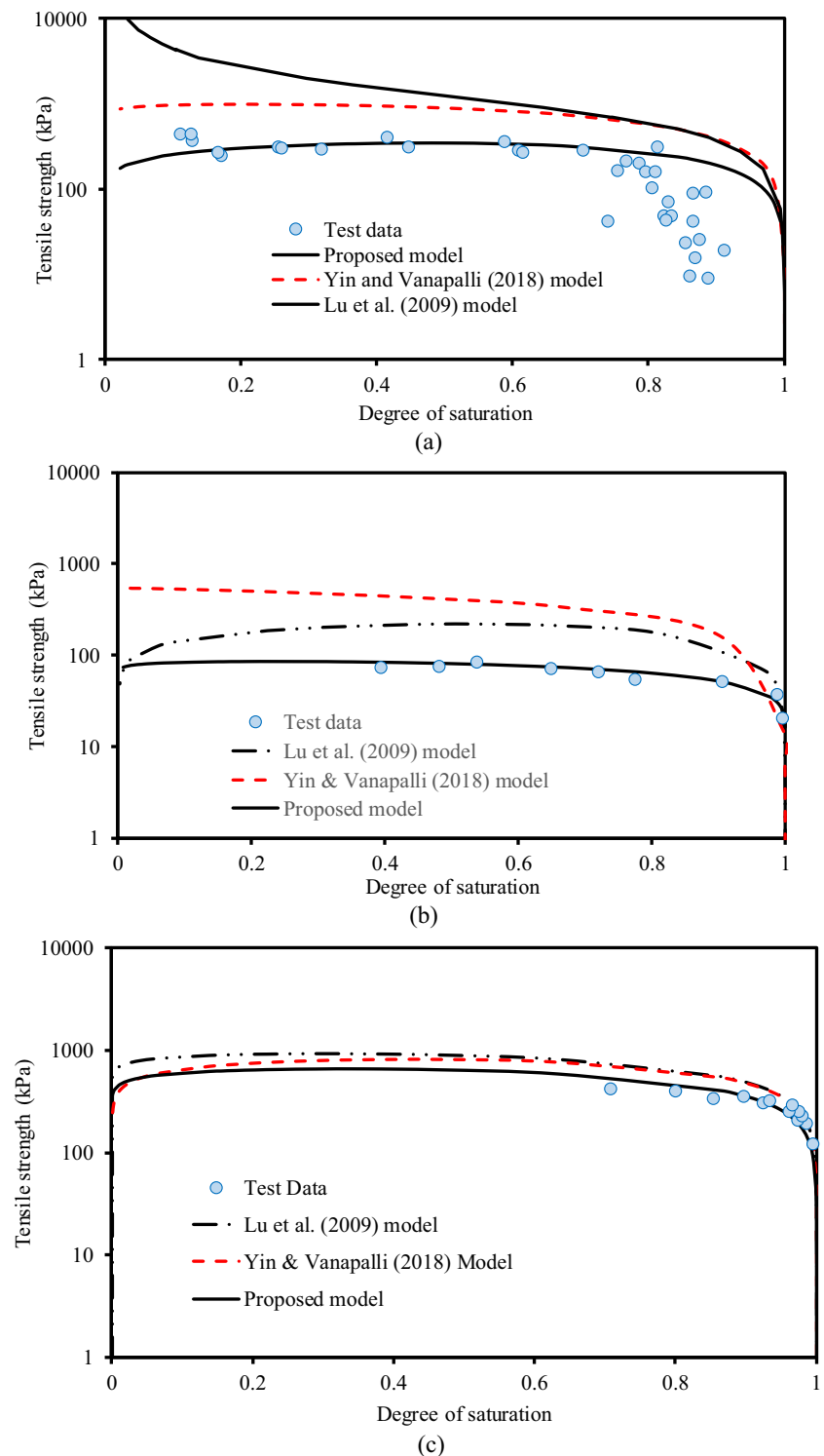
Finally, the coefficients of the regression equations for parameters  $A$  and  $k_{1-2}$  (Eqs. 18 and 19, respectively) were optimized with the calibration dataset to give the final equations, Eqs. 20 and 21, respectively. Note the slight changes in coefficients between Eqs. 18 and 20 for

parameter  $A$ , and between Eqs. 19 and 21 for parameter  $k_1$ .

$$A = -0.395(C_c)^2 + 1.784C_c + 0.041 \tag{20}$$

$$k_1 = 14.115\exp(-1.241n) \tag{21}$$

**Fig. 10** Validation of proposed tensile strength model for fine-grained soils



## Validation

For validation of the proposed tensile strength model, three coarse-grained soils from Win (2006), Kim and Sture (2008), and Jindal et al. (2016) and three fine-grained soils from Zeh and Witt (2005), Wong et al. (2017), and Murray and

Tarantino (2019) were used. These data were not used in the derivation of the proposed tensile strength model. Most important of all, these data are for soils of the same soil structure and contain the SWCC information. The parameters of the validation dataset used in the proposed model are summarized in Table 10. The performances of the modified

tensile strength model, and Lu et al. (2009) and Yin and Vanapalli (2018) models are shown in Figs. 9 and 10 for coarse and fine-grained soils, respectively. The proposed model showed good agreement for the coarse and the fine-grained soils in Figs. 9 and 10 except for Fig. 10a at high degree of saturation (> 80%). The data in Fig. 10a was for a medium plasticity clay which shrinks on drying (Zeh and Witt 2005). For such a soil, it is expected that the soil remains fully saturated as the soil shrinks on drying and only becomes less than fully saturated near the air-entry value. Hence, the data at high degree of saturation were affected by error in the volume measurement. The RMSE for each set of data are shown in Table 11. Figures 9 and 10, and Table 11 show that the proposed tensile strength model outperforms Lu et al.'s (2009) and Yin and Vanapalli's (2018) tensile strength models.

## Conclusion

The present study reviews the macroscopic approach tensile strength models proposed for unsaturated soils. The tensile strength models were proposed for either cohesionless (coarse-grained) or clayey (fine-grained) soils. The differences and discrepancies of the models were highlighted. Brazilian tensile tests were performed on fine-grained soils compacted on the wet side of optimum and subjected to drying at various water contents. Existing tensile strength models for unsaturated soils were not able to model the tensile strength for a wide range of soil types. Using the test data together with data collated from the literature, a new tensile strength model was developed for both unsaturated coarse and fine-grained soils. The proposed model uses the Brazilian tensile test Mohr circle and the extended Mohr–Coulomb criterion. Parameters of the suction stress in the proposed model were related to the grain size distribution and soil–water characteristic curve. Using a validation dataset of three coarse-grained soils and three fine-grained soils, the proposed tensile strength model was shown to perform better than existing tensile strength models.

**Acknowledgments** The first and third authors acknowledge the Singapore International Graduate Award (SINGA) scholarship for this PhD study.

**Authors' contributions** The second author (E.C.L.) contributed to the study conception and design. Data collection and analysis were performed by the first author (S.B.). The manuscript was prepared by S.B. and E.C.L. The third author (R.K.) provided the test data for the fine-grained soils reported in the manuscript.

**Data availability** Available on reasonable request.

## Compliance with ethical standards

**Conflicts of interest/competing interests** The authors declare that they have no competing interests.

## References

- Agus SS, Leong EC, Rahardjo H (2001) Soil–water characteristic curves of Singapore residual soils. *Geotech Geol Eng* 19(3–4):285–309. <https://doi.org/10.1023/A:1013175913679>
- Ajaz A, Parry RHG (1975) Stress–strain behaviour of two compacted clays in tension and compression. *Geotechnique* 25(3):495–512. <https://doi.org/10.1680/geot.1975.25.3.495>
- Akin ID, Likos WJ (2017) Brazilian tensile strength testing of compacted clay. *Geotech Test J* 40(4):608–617. <https://doi.org/10.1520/GTJ20160180>
- Al-Hussaini M (1981) Tensile properties of compacted soils. In: Yong R, Townsend F (eds). *Laboratory shear strength of soil*. ASTM International, West Conshohocken, pp 207–225
- Al-Hussaini MM, Townsend FC (1973) Tensile testing of soils: a literature review. *In Misc paper S73-24*. USAE Waterways Research Station, Vicksburg, Mississippi, pp 36–68
- Alonso EE, Pereira J-M, Vaunat J, Olivella S (2010) A microstructurally based effective stress for unsaturated soils. *Géotechnique* 60(12): 913–925. <https://doi.org/10.1680/geot.8.P.002>
- ASTM D1557-12e1 (2015) Standard test methods for laboratory compaction characteristics of soil using modified effort. West Conshohocken, PA. <https://doi.org/10.1520/D1557-12.1>, [www.astm.org](http://www.astm.org)
- ASTM D3967-16 (2016) Standard test method for splitting tensile strength of intact rock core specimens. West Conshohocken, PA. <https://doi.org/10.1520/D3967-08.2>
- ASTM D4767-11 (2011) Standard test method for consolidated undrained triaxial compression test for cohesive soils. West Conshohocken, PA. <https://doi.org/10.1520/D4767-11.2>
- ASTM D5298-16 (2016) Standard test method for measurement of soil potential (suction) using filter paper. ASTM International, West Conshohocken, PA, 1–6. <https://doi.org/10.1520/D5298-16.2>
- ASTM D6836-16 (2016) Standard test methods for determination of the soil water characteristic curve for desorption using a hanging column, pressure extractor, chilled mirror hygrometer, or centrifuge. West Conshohocken, PA
- ASTM D698 - 12e2 (2015) Standard test methods for laboratory compaction characteristics of soil using standard effort. West Conshohocken, PA. <https://doi.org/10.1520/D0698-12E01>, [www.astm.org](http://www.astm.org)
- Bagge G (1985) Tension cracks in saturated clay cuttings. *Proceedings of 11th international conference on soil mechanics and foundations engineering*, San Francisco, 2:393–395
- Baker R (1981) Tensile strength, tension cracks, and stability of slopes. *Soils Found* 21(2):1–17
- Beckett CTS, Smith JC, Ciancio D, Augarde CE (2015) Tensile strengths of flocculated compacted unsaturated soils. *Geotechnique Letters* 5(4):254–260. <https://doi.org/10.1680/jgele.15.00087>
- Bulut R, Lytton RL, Wray WK (2001) Soil suction measurements by filter paper. *In Proceedings of expansive clay soils and vegetative influence on shallow foundations*, 243–261
- Consoli NC, Festugato L, Consoli BS, Lopes LS (2015) Assessing failure envelopes of soil-fly ash–lime blends. *J Mater Civ Eng* 27(5):1–9. [https://doi.org/10.1061/\(ASCE\)MT.1943-5533.0001134](https://doi.org/10.1061/(ASCE)MT.1943-5533.0001134)
- Das BM, Yen S, Dass R (1995) Brazilian tensile strength test of lightly cemented sand. *Can Geotech J* 32(1):166–171. <https://doi.org/10.1139/t95-013>

- De Souza Villar LF, De Campos TMP, Azevedo RF, Zornberg JG (2009) Tensile strength changes under drying and its correlations with total and matric suctions. *In* Proceedings of the 17th international conference on soil mechanics and geotechnical engineering: the academia and practice of geotechnical engineering. Alexandria, Egypt. pp. 793–796. <https://doi.org/10.3233/978-1-60750-031-5-793>
- Dexter AR, Kroesbergen B (1985) Methodology for determination of tensile strength of soil aggregates. *J Agric Eng Res* 31(2):139–147. [https://doi.org/10.1016/0021-8634\(85\)90066-6](https://doi.org/10.1016/0021-8634(85)90066-6)
- Fahimifar A, Malekpour M (2012) Experimental and numerical analysis of indirect and direct tensile strength using fracture mechanics concepts. *Bull Eng Geol Environ* 71(2):269–283. <https://doi.org/10.1007/s10064-011-0402-7>
- Fisher RA (1926) On the capillary forces in an ideal soil; correction of formulae given by W. B. Haines. *The Journal of Agricultural Science* 16(3):492–505. <https://doi.org/10.1017/S0021859600007838>
- Fredlund DG, Morgenstern NR, Widger RA (1978) The shear strength of unsaturated soils. *Can Geotech J* 15:313–321
- Frydman S (1964) Applicability of the Brazilian (indirect tension) test to soils. *Australian Journal Applied Science* 15(4):335–343
- Frydman S (1967) Triaxial and tensile strength tests on stabilized soil. *In* 3rd Asian regional conference on soil mechanics and foundations engineering. Haifa, 269–275
- Goulding RB (2006) Tensile strength, shear strength, and effective stress for unsaturated sand. University of Missouri, Columbia. <https://doi.org/10.19744/j.cnki.11-1235/f.2006.09.027>
- Hasegawa H, Ikeuti M (1966) On the tensile strength test of disturbed soils. *In* Rheology and soil mechanics / Rhéologie et Mécanique des sols. Edited by P. Kravtorenco, J. and Sirieys and M. Springer, Berlin, Heidelberg. pp. 405–412. [https://doi.org/10.1007/978-3-662-39449-6\\_33](https://doi.org/10.1007/978-3-662-39449-6_33)
- He S, Bai H, Xu Z (2018) Evaluation on tensile behavior characteristics of undisturbed loess. *Energies* 11(8):1–18. <https://doi.org/10.3390/en11081974>
- Iraivanian A, Bilsel H (2016) Tensile strength properties of sand–bentonite mixtures enhanced with cement. *Procedia engineering*, 143(ctg): 111–118. Elsevier B.V. <https://doi.org/10.1016/j.proeng.2016.06.015>
- Jindal P, Sharma J, Bashir R (2016) Effect of pore-water surface tension on tensile strength of unsaturated sand. *Indian Geotechnical Journal* 46(3):276–290. <https://doi.org/10.1007/s40098-016-0184-8>
- Kennedy TW, Hudson WR (1968) Application of the indirect tensile test to stabilized materials. Highway Research Board. Available from <http://onlinepubs.trb.org/Onlinepubs/hr/1968/235/235-004.pdf>
- Krishnayya AV, Eisenstein Z (1974) Brazilian tensile test for soils. *Can Geotech J* 11(4):632–642. <https://doi.org/10.1139/t74-064>
- Kim T, Kim T, Kang G, Ge L (2012) Factors influencing crack-induced tensile strength of compacted soil. *J Mater Civ Eng* 24(3):315–320. [https://doi.org/10.1061/\(ASCE\)MT.1943-5533.0000380](https://doi.org/10.1061/(ASCE)MT.1943-5533.0000380)
- Kizza R (2019) Suction, hydraulic and strength properties of compacted soils. Nanyang Technological University, Singapore
- Kim TH, Hwang C (2003) Modeling of tensile strength on moist granular earth material at low water content. *Eng Geol* 69(3–4):233–244. [https://doi.org/10.1016/S0013-7952\(02\)00284-3](https://doi.org/10.1016/S0013-7952(02)00284-3)
- Kim TH, Sture S (2008) Capillary-induced tensile strength in unsaturated sands. *Can Geotech J* 45(5):726–737. <https://doi.org/10.1139/T08-017>
- Kim B, Shibuya S, Park S, Kato S (2010) Application of suction stress for estimating unsaturated shear strength of soils using direct shear testing under low confining pressure. *Can Geotech J* 47(9):955–970
- Leong EC, Wijaya M (2015) Universal soil shrinkage curve equation. *In*: *Geoderma*, 237: 78–87. Elsevier, B.V. <https://doi.org/10.1016/j.geoderma.2014.08.012>
- Leong E, He L, Rahardjo H (2002a) Factors affecting the filter paper method for total and matric suction measurements. *Geotech Test J* 25(3):1–12. <https://doi.org/10.1520/GTJ11094J>
- Leong EC, Rahardjo H, Tang SK (2002b) Characterisation and engineering properties of Singapore residual soils. *In* Proceedings of the international workshop on characterisation and engineering properties of natural soils, Singapore, 2:1279–1304
- Leong E, Tripathy S, Rahardjo H (2003) Total suction measurement of unsaturated soils with a device using the chilled-mirror dew-point technique. *Géotechnique* 53(2):173–182
- Li D, Wong LNY (2013) The Brazilian disc test for rock mechanics applications: review and new insights. *Rock Mech Rock Eng* 46(2):269–287
- Li HD, Tang CS, Cheng Q, Li SJ, Gong XP, Shi B (2019) Tensile strength of clayey soil and the strain analysis based on image processing techniques. *Engineering Geology*, 253:137–148. Elsevier. <https://doi.org/10.1016/j.enggeo.2019.03.017>
- Lu N, Wu B, Tan CP (2007) Tensile strength characteristics of unsaturated sands. *J Geotech Geoenviron* 133(2):144–154. [https://doi.org/10.1061/\(ASCE\)1090-0241\(2007\)133:2\(144\)](https://doi.org/10.1061/(ASCE)1090-0241(2007)133:2(144))
- Lu N, Kim T-H, Sture S, Likos WJ (2009) Tensile strength of unsaturated sand. *J Eng Mech* 135(12):1410–1419. [https://doi.org/10.1061/\(ASCE\)EM.1943-7889.0000054](https://doi.org/10.1061/(ASCE)EM.1943-7889.0000054)
- Mendes J (2011) Assessment of the impact of climate change on an instrumented embankment: an unsaturated soil mechanics approach. Durham theses. Durham University. Available from online: <http://etheses.dur.ac.uk/612/>
- Morris PH, Graham J, Williams DJ (1992) Cracking in drying soils. *Can Geotech J* 29(2):263–277. <https://doi.org/10.1139/t92-030>
- Munkholm LJ, Kay BD (2014) Effect of water regime on aggregate-tensile strength, rupture energy, and friability. *Soil Sci Soc Am J* 66(3):702. <https://doi.org/10.2136/sssaj2002.7020>
- Murray I, Tarantino A (2019) Mechanisms of failure in saturated and unsaturated clayey geomaterials subjected to (total) tensile stress. *Geotechnique* 69(8):701–712. <https://doi.org/10.1680/jgeot.17.P.252>
- Narvaez B, Aubertin M, Saleh-Mbemba F (2015) Determination of the tensile strength of unsaturated tailings using bending tests. *Can Geotech J* 52(11):1874–1885. <https://doi.org/10.1139/cgj-2014-0156>
- Peters J, Leavell D (1988) Relationship between tensile and compressive strengths of compacted soils. *In*: Donaghe RT, Chancy RC, Silver ML (eds) *Advanced triaxial testing of soil and rock*, ASTM STP 9. American Society for Testing and Materials, Philadelphia, pp 169–188. <https://doi.org/10.1520/stp29077s>
- Pittaro G (2019) Tensile strength behaviour of ground improvement and its importance on deep excavations using deep soil. *In* XVII European conference on soil mechanics and geotechnical engineering. pp. 1–8. <https://doi.org/10.32075/17ECSMGE-2019-0085>
- Shi B, Chen S, Han H, Zheng C (2014) Expansive soil crack depth under cumulative damage. *The Scientific World Journal* 2014:1–9. <https://doi.org/10.1155/2014/498437> research
- Sivakugan N, Das BM, Lovisa J, Patra CR (2014) Determination of  $c$  and  $\Phi$  of rocks from indirect tensile strength and uniaxial compression tests. *Int J Geotech Eng* 8(1):59–65. <https://doi.org/10.1179/1938636213Z.00000000053>
- Snyder VA, Miller RD (1985) Tensile strength of unsaturated soils. *Soil Sci Soc Am J* 49(1):58–65. <https://doi.org/10.2136/sssaj1985.03615995004900010011x>
- Tang GX, Graham J (2000) A method for testing tensile strength in unsaturated soils. *Geotech Test J* 23(3):377–382. <https://doi.org/10.1520/gtj11059j>
- Tang CS, Pei XJ, Wang DY, Shi B, Li J (2015) Tensile strength of compacted clayey soil. *Journal of Geotechnical and Geoenvironmental Engineering*, 141(4):04014122\_ 1–8. [https://doi.org/10.1061/\(ASCE\)GT.1943-5606.0001267](https://doi.org/10.1061/(ASCE)GT.1943-5606.0001267)



- Tang L, Zhao Z, Luo Z, Sun Y (2019) What is the role of tensile cracks in cohesive slopes? *Journal of rock mechanics and geotechnical engineering*, 11(2):314–324. Elsevier Ltd. <https://doi.org/10.1016/j.jrmge.2018.09.007>
- Tarantino A (2010) Unsaturated soils: compacted versus reconstituted states. *In* 5th international conference on unsaturated soil. Barcelona, pp 113–136. <https://doi.org/10.1201/b10526-9>
- Trabelsi H, Jamei M, Guiras H, Hatem Z, Romero E, Sebastia O (2010) Some investigations about the tensile strength and the desiccation process of unsaturated clay. *EPJ Web of Conferences* 6:12005. <https://doi.org/10.1051/epjconf/20100612005.i>
- Trabelsi H, Jamei M, Zenzri H, Olivella S (2012) Crack patterns in clayey soils: experiments and modeling. *Int J Numer Anal Methods Geomech* 36(11):1410–1433. <https://doi.org/10.1002/nag.1060>
- Tschebotarioff G, Ward E, Dephippe A (1953) The tensile strength of disturbed and recompacted soils. *In* 3rd international conference on soil mechanics and foundation engineering. Switzerland, 207–210
- Uchida I, Matsumoto R (1961) On the test of the modulus of rupture of soil sample. *Soils Found* 2(1):51–55. Available from <http://www.mendeley.com/research/geology-volcanic-history-eruptive-style-yakedake-volcano-group-central-japan/>
- Van Genuchten MT (1980) A closed-form equation for predicting the hydraulic conductivity of unsaturated soils. *Soil Sci Soc Am J* 44(5):892–898
- Vanicek I (2013) The importance of tensile strength in geotechnical engineering. *Acta Geotechnica Slovenica* 10(1):5–17. [https://doi.org/10.1016/0022-2836\(71\)90334-2](https://doi.org/10.1016/0022-2836(71)90334-2)
- Varsei M, Miller GA, Hassanikhah A (2016) Novel approach to measuring tensile strength of compacted clayey soil during desiccation. *International Journal of Geomechanics* 16(6):D4016011. [https://doi.org/10.1061/\(asce\)gm.1943-5622.0000705](https://doi.org/10.1061/(asce)gm.1943-5622.0000705)
- Vesga L, Vallejo L (2006) Direct and indirect tensile tests for measuring the equivalent effective stress in a kaolinite clay. *In* Fourth international conference on unsaturated soils. Carefree, Arizona, United States, pp. 1290–1301
- Wang JP, François B, Lambert P (2020) From basic particle gradation parameters to water retention curves and tensile strength of unsaturated granular soils. *International Journal of Geomechanics* 26(6):1–10. [https://doi.org/10.1061/\(ASCE\)GM.1943-5622.0001677](https://doi.org/10.1061/(ASCE)GM.1943-5622.0001677)
- Win SS (2006) Tensile strength of compacted soils subjected to wetting and drying. The University of New South Wales Sydney, Australia
- Wong CK, Wan RG, Wong RCK (2017) Tensile and shear failure behaviour of compacted clay – hybrid failure mode. *International journal of geotechnical engineering*, 6362(December):1–11. Taylor & Francis. <https://doi.org/10.1080/19386362.2017.1408242>
- Yin P, Vanapalli SK (2018) Model for predicting tensile strength of unsaturated cohesionless soils. *Can Geotech J* 55(9):1313–1333. <https://doi.org/10.1139/cgj-2017-0376>
- Young JF (1967) Humidity control in the laboratory using salt solutions—a review. *J Appl Chem* 17(9):241–245. <https://doi.org/10.1002/jctb.5010170901>
- Zeh R, Witt K (2005) Suction-controlled tensile strength of compacted clays. *In* Proceedings of international conference on soil mechanics and geotechnical engineering. pp. 2347–2350